Starvation-dependent regulation of eIF6 through multisite phosphorylation by GSK3β

Courtney F. Jungers[1], Jonah M. Elliff[1], Daniela S. Masson-Meyers[1], Christopher J. Phiel[2], Sofia Origanti[1]

1. Department of Biological Sciences, Marquette University, Milwaukee, WI - 53233, USA
2. Department of Integrative Biology, University of Colorado Denver, Denver, CO - 80217, USA

Running Title: Regulation of eIF6 by GSK3β

Corresponding Author: Sofia Origanti, 530N 15th St., Wehr Life Sciences, Department of Biological Sciences, Marquette University, Milwaukee, WI-53233, Ph: 414-288-7286, sofia.origanti@marquette.edu

Abstract

Eukaryotic translation initiation factor 6 is essential for the synthesis of 60S ribosomal subunits and for regulating the association of 60S and 40S ribosomal subunits. A mechanistic understanding of how eIF6 modulates protein synthesis in response to stress, specifically starvation-induced stress, is lacking. Our studies have uncovered a novel mode of eIF6 regulation by Glycogen Synthase Kinase-3 that is predominantly active in response to serum starvation. Human eIF6 is phosphorylated by GSK3β at a multisite motif in the C-terminal tail. Robust and sequential phosphorylation by GSK3β requires phosphorylation at a priming site. In response to serum starvation, eIF6 accumulates in the cytoplasm and this altered subcellular localization is dependent on GSK3 activity. These results suggest that eIF6 regulation by GSK3β could contribute to the attenuation of global protein synthesis that is critical for adaptation to starvation-induced stress.

Key words: eIF6/GSK3β/Phosphorylation/Starvation/Translation

Introduction

Eukaryotic initiation factor 6 (eIF6) is a key modulator of translation initiation that regulates the biogenesis and availability of the 60S ribosomal subunits[1-3]. eIF6 directly associates with pre-60S complexes in the nucleolus and is exported into the cytoplasm in complex with the 60S where it aids in 60S maturation[4-8]. The well-characterized role of eIF6 is its anti-association activity that prevents interactions between the 60S and 40S ribosomal subunits[2,9-12]. Structural and biochemical studies indicate that eIF6 binds to 60S at the 40S-binding interface and sterically hinders association of the 40S subunits[10-16]. Release of eIF6 from the mature 60S allows association of the 40S-mRNA complex, which leads to active 80S formation and translation initiation[10-15]. An inhibition of eIF6 release (or premature release) from the 60S subunits can greatly influence intersubunit association and translation initiation. A block in eIF6 release leads to an increase in the fraction of eIF6-bound 60S subunits that are unable to join 40S, which hinders the assembly of active 80S monosomes[10-13,15,16]. Alternatively, insufficient levels of eIF6 lead to spurious association of 60S with the 40S subunits that are devoid of mRNA. This causes an increase in the assembly of inactive 80S monosomes, which impairs translational response to growth stimuli as seen in *eIF6*+/- mice[17-19]. Thus, an impairment of eIF6 function or levels can substantially limit protein synthesis specifically in response to growth stimuli, and this deregulation has been shown to contribute to the underlying pathologies of diseases such as Shwachman-Bodian-Diamond syndrome, cancer and certain metabolic disorders[13,17-20].

In response to growth stimuli such as insulin or phorbol esters, primary hepatocytes and mouse embryonic fibroblasts (MEFs) derived from the *eIF6*+/- mice do not upregulate protein synthesis unlike the wild type (WT) cells[17-19]. Similar defects in translation are also observed *in vivo,* where livers of *eIF6*+/- mice are smaller, and exhibit an accumulation of inactive/empty (mRNA-free) 80S ribosomes compared to WT[17-19]. The lack of insulin-dependent stimulation of protein synthesis in the *eIF6*+/- mice has been associated with a reprogramming of fatty acid synthesis and glycolytic pathways with implications for muscle, liver and fat metabolism[19,21].

In terms of mechanism, the increased formation of inactive 80S complexes in the *eIF6*+/- cells is

attributed to an impairment of its anti-association function in the cytoplasm[17-19]. Interestingly, such an accumulation of inactive 80S monosomes is commonly observed in cells subjected to stress, especially stress induced by nutrient deprivation or limitation[22-24]. Starvation or nutrient limitation in yeast and mammalian cells invokes an adaptive metabolic response that conserves energy by restricting global protein synthesis and leads to an accumulation of inactive (empty) 80S ribosomes along with an inhibition of ribosome biogenesis[22-31]. The mechanisms that contribute to the accumulation of the empty 80S ribosomes in response to starvation and the role of eIF6 as a ribosome anti-association and ribosome biogenesis factor in modulating this response have not been thoroughly explored. Given the key role of eIF6 in regulating translational response to insulin and growth factors in an mTOR-independent manner[19,32], it is important to understand the mechanisms that control eIF6 in response to growth inhibitory stress responses. Towards addressing this, here we report a novel regulation of eIF6 by the Glycogen Synthase Kinase-3 (GSK3) that is active under conditions of starvation-induced stress and may contribute to the formation of inactive 80S complexes.

Global proteomic and biochemical studies indicate that eIF6 is phosphorylated at multiple sites and majority of these sites are conserved and cluster around the C-terminal tail[33-39]. However, most of these phosphorylation sites have not been validated *in vivo* and the identity of the associated kinases have not been clarified. It is also unclear if these uncharacterized phosphorylation sites carry any functional relevance. Therefore, we carried out a sequence analysis and identified a putative motif for GSK3 phosphorylation within the C-terminal tail of eIF6. Previous studies show that GSK3 is uniquely activated in response to growth inhibitory conditions such as starvation or quiescence and is inhibited in response to insulin and other growth stimulatory conditions by AKT and mTORC1/p70S6K1-dependent phosphorylation[40-46]. GSK3 plays a prominent role in translational control by inhibiting the nucleotide exchange function of the translation initiation factor: eIF2B, which is reversed in response to insulin[40,47-49]. GSK3 phosphorylates the Ser-540 site in the epsilon subunit of eIF2B to inhibit its activity[40,47-49]. Here, we show that GSK3 also regulates eIF6 by phosphorylating human eIF6 *in* vitro on a multisite motif. We also show that GSK3 interacts with endogenous eIF6 *in vivo* and phosphorylation by GSK3β alters the subcellular localization of eIF6 in response to serum starvation. One of the residues of phosphorylation was identified as S235, and S235

phosphorylation has been previously shown to prevent eIF6 association with the 60S ribosome[12,17]. Based on the finding that eIF6 is a novel substrate of GSK3 we propose a model wherein GSK3-dependent phosphorylation of eIF6 contributes to translation inhibition in response to starvation by regulating eIF6 function in 60S/40S subunit joining and/or 60S biogenesis.

Results

The C-terminal tail of eIF6 is phosphorylated by GKS3β

Sequence analysis of the amino acid residues in the C-terminal tail of human eIF6 revealed the presence of sequential S/TXXXS/T motifs as potential candidates for phosphorylation by GSK3. We identified two such multisite motifs (motif 1 and 2) in the C-terminus that are highly conserved in higher eukaryotes from *Xenopus* to mammals (Fig. 1A) but show variability in lower eukaryotes such as yeast. GSK3 phosphorylates residues on its substrates in a sequential manner starting with the C-terminus, and for a majority of substrates, GSK3 works in concert with a priming kinase that phosphorylates a priming site located 3 residues away from the GSK3 recognition site (Fig. 1A)[40,42,43,50-52]. The potential priming sites are indicated in Fig. 1A. To determine if eIF6 is a substrate of GSK3, we immunoprecipitated eIF6 from HCT116 cells that were briefly serum-starved to ensure that GSK3 and any associated priming kinase were sufficiently activated. For the kinase assays, we used immunoprecipitated eIF6 instead of recombinant eIF6 purified from *E. coli,* as the pure protein is not expected to be in a primed state, and it was unclear if priming of eIF6 was a requisite for phosphorylation by GSK3. Also, we focused on the GSK3β isoform in this study, which is the well characterized isoform[41]. We confirmed that GSK3β was sufficiently activated in response to short-term serum-starvation in HCT116 cells by probing for the loss of the inhibitory phosphorylation of the serine-9 residue. The serine-9 site on GSK3β is phosphorylated by kinases such as AKT, and the phosphorylated N-terminal end acts as a pseudo substrate to inhibit GKS3β activity[41,43-46,50,51]. Therefore, a loss of S9 phosphorylation indicates activation of GSK3β as seen during serum-starvation (Fig. S1A, B).

We then determined if the immunoprecipitated eIF6 is directly phosphorylated by recombinant GSK3. Our results show that eIF6 is indeed phosphorylated by GSK3β *in vitro* and

phosphorylation was found to be specific since we did not observe a similar phosphorylated form in the empty vector control lanes (Fig. 1B). We also observed autophosphorylation of GSK3β, which has been reported before[42]. We observed a doublet of immunoprecipitated myc-eIF6 in the western blot and this upward shift or slower migration is highly likely to represent a post-translationally modified form owing to the experimental condition of short-term serum starvation. The intensity of the doublet was found to be quite variable between experiments and was not cell-type specific (Fig. 3A). The doublet is unlikely to be a cleavage product since the myc-tag antibody that recognizes the N-terminus and the eIF6 antibody that is specific to the C-terminal tail were able to detect both bands. Analysis of the *in vitro* kinase assay also revealed two phosphorylated forms of eIF6 suggesting that there is a basal and hyperphosphorylated form induced by GSK3. We further tested for specificity by eliminating the two multisite motifs in the C-terminus by creating a deletion mutant that lacks the last 36 amino acid residues (eIF6-CΔ36). GSK3β did not phosphorylate eIF6-CΔ36 whereas it phosphorylated the full-length eIF6 suggesting that the last 36 residues are critical for phosphorylation (Fig. 1C). We did observe a faint phosphorylated form in the eIF6-CΔ36 lane, which could indicate some non-specific phosphorylation observed in the absence of sites that are specific to the kinase or associated with the light chain of the myc-antibody found in the immunoprecipitated sample (Fig. 1C). Prolonged exposures of the blots have captured a similar non-specific band in the myc-empty vector lane incubated with the kinase (Fig. S3A).

GSK3β phosphorylates multiple sites within the last 20 amino acid residues of eIF6

To identify the specific residues phosphorylated by GSK3β, we carried out nanoscale liquid chromatography with tandem mass spectrometry analysis (*nano*LC-MS/MS) on the immunoprecipitated eIF6 sample incubated with and without GSK3β. MS analysis revealed that the T231 residue was phosphorylated in the sample incubated with GSK3β (Fig. 1D, S2C, D). The relative abundances of the peptides in the samples incubated with and without the kinase were found to be identical (Fig. S2A, B). However, we were unable to detect other sites of phosphorylation among the last 36 residues in the C-terminal tail. It is highly likely that the technical limitations associated with our MS analysis, and low sample abundance that stemmed from using immunoprecipitated eIF6 as opposed to purified recombinant protein limited the detection of phosphopeptides carrying two or more phosphorylated residues. Phosphorylation of

the T231 residue indicated that motif-2 in the C-terminal tail is likely to be phosphorylated by GSK3β. Motif-2 is in the disordered region of the C-terminal tail of eIF6 that is predicted to protrude outside the core structure, which would be favorable for regulatory interactions[10,16]. Also, all the predicted sites indicated in motif-2 were previously identified to be modified by phosphorylation in global proteomic studies including those performed under cellular conditions of stress[33-39]. Furthermore, previous studies did not detect phosphorylated residues in motif-1 of mammalian eIF6 (PhosphoSitePlus). To test if motif-2 is critical for recognition by GSK3β, a deletion mutant lacking the last 20 residues in the C-terminal tail (eIF6-CΔ20) was generated. Indeed, deletion of just motif-2 greatly reduced eIF6 phosphorylation, which in combination with the MS analysis indicated that the sites of phosphorylation are in motif-2 (Fig. 2A).

To further identify the specific sites of phosphorylation in motif-2, we generated phospho-site mutants where individual serine or threonine residues within motif-2 were substituted with alanine (Fig. 2B). Interestingly, substitution of the potential priming site serine-243 with alanine resulted in a significant 40% reduction in phosphorylation in comparison to the wild type eIF6 (eIF6-FL) (Fig. 2C, S3B). This suggested that in the absence of the S243 priming site, the S239, S235 and T231 sites are phosphorylated, however priming phosphorylation at S243 is required for efficient phosphorylation of eIF6. To determine if the other three sites are phosphorylated in a GSK3-specific manner, we generated a 3A phospho-site version carrying the following serine to alanine substitutions: T231A, S235A, S239A (Fig. 2B). In the absence of the T231, S235 and S239 sites, phosphorylation of eIF6 was greatly reduced with a complete loss of the hyperphosphorylated form suggesting that these are the key sites of phosphorylation (Fig. 2C). The loss of the eIF6 doublet that we normally see with the eIF6-FL protein in the autoradiograph (Fig. 1B, C) clearly suggests that the higher band is a hyperphosphorylated version. Similar results were obtained with the 4A mutant wherein all 4 sites were substituted with alanine, suggesting that all the four residues are key for phosphorylation by GSK3β and that S243 is the potential priming site (Fig. 2C).

GSK3β phosphorylates multiple sites on eIF6 in a sequence

In the presence of multiple and adjacent recognition sites, GSK3 phosphorylates residues in a sequence starting from the C-terminus. Examples of sequential phosphorylation include

substrates such as β-catenin and glycogen synthase that carry 3 and 4 GSK3-specific sites respectively[53-57]. To determine if phosphorylation of eIF6 is also sequential, we generated single phospho-site mutants where the respective threonine or serine residues were mutated to alanine (Fig. 2D). Substitution of serine-239 (first GSK3-specific site in the sequence) with alanine greatly reduced eIF6 phosphorylation and resulted in a complete loss of the hyperphosphorylated form. Similar results were obtained with the S235A mutation that disrupted the second site in the sequence. The S235A mutant also displayed a marked reduction in phosphorylation and showed a complete loss of the hyperphosphorylated form (Fig. 2D). The presence of basal phosphorylation in the S235A mutant could indicate phosphorylation of the S239 site, which is the first GSK-3 specific site in the sequence. Some basal phosphorylation was also observed with the S239A site mutant, which could be due to non-priming dependent phosphorylation of one of the other sites in the sequence (Fig. 2D). However, in both these cases, a complete absence of the hyperphosphorylated form indicates that mutations of the first and second residue in the sequence disrupt hyperphosphorylation of eIF6. We further tested the effect of mutating the T231 site, which is the last phospho-site in the sequence. Interestingly, the T231A mutant retained the hyperphosphorylated form, however, it exhibited an overall 40% reduction in phosphorylation relative to wild type eIF6 (Fig. 2D, S3C). This suggested that the S239 and S235 sites, the first two sites in the sequence are phosphorylated even in the absence of the last T231 residue and could account for a significant fraction of the hyperphosphorylated form. However, the overall decrease in phosphorylation in the absence of the T231 site suggests that the T231 site is also a key site phosphorylated by GSK3β. These results indicate that the phosphorylation of eIF6 is sequential.

We further validated the sequential phosphorylation by carrying out MS analysis on a phosphopeptide incubated with GSK3β *in vitro*. The phosphopeptide was designed to carry a phosphate group on the S243 site (putative priming site) to mimic a primed state (Fig. 2E). MS analysis revealed that GSK3β phosphorylated a major fraction of the peptides at the S239 site, the first site in the sequence. Also, a very small fraction of phosphopeptide was phosphorylated at both the S235 and S239 sites (Fig. 2E, S3D). It was technically challenging to detect quadruple phosphorylated peptides that were phosphorylated at all three GSK3-specific sites (S239, S235, T231) along with the S243-priming site (Fig. 2E). However, since the T231 site

was identified earlier using our previous MS analysis on immunoprecipitated eIF6, which in combination with the single-site mutant analysis, validated the T231 site as one of the sites phosphorylated by GSK3 (Fig. 1D). Interestingly, we were unable to detect any peptides that were phosphorylated by GSK3 at just the S235 or T231 sites, which further suggested that the multisite phosphorylation of eIF6 by GSK3 occurs in a sequence. These MS results in combination with single-site mutant analyses strongly suggested that the phosphorylation of eIF6 by GSK3β is in a sequence starting with the S239 site, followed by the S235 site and ending with the T231 site.

Priming is critical for robust phosphorylation of eIF6

Analysis of the eIF6 priming site mutant (S243A) indicated that in the absence of priming, phosphorylation by GSK3β is significantly reduced (Fig. 2C). We further ascertained the need for priming by performing the kinase assay with a mutant of GSK3β (R96A) that is unable to phosphorylate substrates that require priming[43,50,51]. The arginine-96 to alanine substitution in GSK3β disrupts the priming recognition site within the kinase[43,50]. Substrates that are primed by phosphorylation, dock on to this priming recognition site followed by phosphorylation at the catalytic site[43,50]. However, substrates that do not require priming are phosphorylated by the R96A mutant with efficiency similar to the wild type GSK3β[43,50,51]. In our experiments, as expected, wild-type GST-GSK3 phosphorylated eIF6 and displayed both the basal and hyperphosphorylated forms (Fig. 3A). However, no such doublet was observed with the GST-GSK3-R96A mutant suggesting that recognition of the primed phosphorylation is critical for efficient phosphorylation of eIF6 (Fig. 3A).

GSK3 interacts with endogenous eIF6 in human cells

We next tested if GSK3β interacts with eIF6 in human cells. Due to the transient nature of kinase-substrate interactions, we ectopically expressed GST-GSK3β in HCT116 cells. GST-GSK3β pulled-down from HCT116 cells was found to interact with endogenous eIF6 (Fig. 3B, C). The interaction was found to be specific to GSK3β as no such interaction was observed with either empty vector or GST alone (Fig. 3B, C). We also observed that the total levels of eIF6 were not altered by overexpression of GST-GSK3β, suggesting that GSK3β may not regulate the total protein levels. This was also confirmed by probing for eIF6 protein levels in response to

long-term serum-starvation when GSK3β is fully active (Fig. S1A, B.). We did not detect significant changes in total eIF6 protein levels even after 18 hours of starvation suggesting that GSK3β may not regulate the stability or synthesis of eIF6 protein (Fig. 3D, E).

Altered sub-cellular localization of eIF6 in response to starvation is regulated by GSK3

Since the total levels of eIF6 were unaltered, we next tested whether GSK3β regulates eIF6 function by altering its subcellular localization. We also tested if long-term serum starvation that correlates with full activation of GSK3β altered the subcellular localization of eIF6. Immunofluorescence staining of endogenous eIF6 showed that eIF6 localization to the cytoplasm was enhanced in response to serum starvation in HCT116 cells (Fig. 4A). These results were further confirmed by using a different monoclonal antibody specific for eIF6, which ruled out non-specific staining associated with the antibody (Fig. S4A). This is the first evidence of localization-specific regulation of eIF6 in response to starvation-induced stress. To further determine if this altered sub-cellular localization was dependent on GSK3 activity, cells were treated for a short-term with CHIR99021 and SB415286, two highly selective GSK3-specific inhibitors[58,59]. The potency of the GSK3-specific inhibitors was validated by probing for a loss of phosphorylation of β-catenin at GSK3-specific sites (S33/S37/T41)[53-55,60]. Short-term treatment with both the inhibitors resulted in greater than 50% loss in β-catenin phosphorylation suggesting that GSK3 is inhibited under these conditions (Fig. S4B, C). In cells treated with the GSK3 inhibitors, a partial rescue of eIF6 localization to the nucleus was observed (Fig. 4A).

We further quantitated eIF6 levels in the nuclear and cytoplasmic fractions by subcellular fractionation. The purity of different fractions was confirmed by probing for Topoisomerase IIβ, a nuclear marker and αTubulin, a cytoplasmic marker. eIF6 was distributed almost equally between the nuclear and cytoplasmic fractions in serum-fed controls (53% nucleus, 47% cytoplasm), and no significant difference was found between the two fractions (Fig. 4B, S5C). Similar to the imaging results, we found that in the serum-starved cells there was a significant decrease in eIF6 levels in the nucleus with a corresponding increase in the cytoplasm (~32-33% in nucleus, ~67-68% in cytoplasm) (Fig. 4B, 4C, S5D, S5E). Inhibition of GSK3 completely restored the nuclear-cytoplasmic distribution as seen in the CHIR990021-treated cells (54% nucleus, 46% cytoplasm) (Fig. 4C, S5F). No differences were observed between the total input

levels of eIF6 under all conditions tested (Fig. S5A, B). Similar results were also found in a normal rat intestinal epithelial cell line (RIE-1) where eIF6 shows cytoplasmic accumulation in response to serum-starvation, which is reversed by inhibition of GSK3 (Fig. 5A). These results strongly suggest that eIF6 exhibits cytoplasmic accumulation in response to serum-starvation and this response is regulated by GSK3.

Discussion

The metabolic response to starvation is to conserve energy and limit processes with high energy requirements such as translation and ribosome biogenesis[22-31]. Here, we provide a novel link between starvation response and regulation of both translation initiation and ribosome biogenesis through the control of translation initiation factor eIF6. Despite its extensive role in metabolism, eIF6 function in starvation-response is poorly understood. We show for the first time that eIF6 is regulated in response to starvation-induced stress and that the regulation hinges on the GSK3 signaling pathway that is prolifically active under such nutrient-deprived conditions. This study also identifies GSK3 as one of the kinases that phosphorylates the multiple sites in the C-terminal tail of eIF6. Although several studies have shown that the C-terminal tail of eIF6 is heavily phosphorylated, the identity of the kinases involved, other than PKCβII, were largely unknown[12]. Our results show that GSK3 sequentially phosphorylates the C-terminal tail of eIF6 on three sites (S239, S235, and T231) and efficient phosphorylation of these sites requires priming at S243. It is currently unclear as to which priming kinase works in concert with GSK3 and the identity and functional significance of this priming kinase will be investigated in future studies.

Interestingly, the S235 site is also phosphorylated by the RACK1-PKCβII complex[12]. Biochemical studies show that the RACK1-PKCβII-dependent phosphorylation of eIF6 results in its release from the 60S subunits and enables active 80S formation[12]. Substitution of the serine-235 site with alanine blocks eIF6 release and inhibits active 80S formation[12]. Apart from *in vitro* studies, the S235 site has also been shown to be important for normal growth and translation *in vivo*[17,18]. Studies in *eIF6*+/- MEFs reconstituted with the S235A mutant show that the S235 site is critical for eIF6 function in stimulating translation in response to insulin and phorbol esters[17-19]. It is not uncommon for a single site to be regulated by multiple kinases in a context-dependent

manner. Since PKCβII is active under conditions of growth and proliferation, whereas GSK3 is active under growth-deprived conditions, it is likely that these two kinases phosphorylate the S235 site based on the polarizing cellular cues of growth and starvation. Regardless of the identity of the kinase, phosphorylation at the S235 site is expected to exert a similar effect and inhibit eIF6 association with the ribosome. However, in the case of eIF6 phosphorylation by GSK3β, additional sites are also phosphorylated, which would further structurally perturb the local protein structure. The functional significance of sequential and multi-site phosphorylation will have to be established.

We observe enhanced cytoplasmic accumulation of eIF6 in response to serum-starvation and the altered localization is reversed by GSK3 inhibition. Since GSK3 is predominantly cytoplasmic with a small nuclear fraction[40], it is likely that phosphorylation by GSK3 leads to increased cytoplasmic retention of eIF6. A previous report in COS-7 cells indicates that the percentage of eIF6 in the cytoplasm is ~70% compared to the ~50% distribution that we observe in HCT116 cells[61]. It is likely that the exact percentages in terms of eIF6 distribution may vary based on the cell type. However, the increased accumulation of eIF6 in response to starvation was consistently observed among different cell lines including the normal RIE-1 cells. A previous study showed that the nuclear import of eIF6 was mediated by calcium-activated calcineurin phosphatase whereas the nuclear export was mediated by phosphorylation of eIF6 at S174/175 residues by nuclear casein kinase1 in COS-7 cells[61]. However, these studies were not carried out under conditions of serum starvation or nutrient deprivation. Thus, our results and previous data suggest that varying the subcellular localization of eIF6 may be a predominant mode of regulating eIF6 function, and the underlying signaling mechanisms may vary based on the growth stimulus and stressed states.

Based on these results, we propose a model of eIF6 regulation in response to starvation (Fig. 5B). Under nutrient or growth-limiting conditions, AKT and mTORC1-p70S6K signaling mechanisms are inactivated, which in turn activates GSK3 (Fig. 5B). Activation of GSK3 in concert with a priming kinase leads to phosphorylation of eIF6 at four sites. Phosphorylation by GSK3 leads to increased cytoplasmic accumulation of eIF6. It is likely that the cytoplasmic retention of eIF6 inhibits its nucleolar functions in 60S biogenesis and contributes to the

inhibition of ribosome biogenesis that is observed during starvation. The multisite phosphorylation of eIF6 including the S235 site is expected to prevent eIF6 association with the ribosome. This could lead to spurious association of the 60S subunits with the 40S subunits and lead to the empty 80S accumulation that is observed in response to starvation-induced stress. Thus, phosphorylation of eIF6 could control availability of the 60S ribosomal subunits, which in concert with other signaling mechanisms such as the inhibition of the mTOR complex and GSK3-dependent inhibition of eIF2B could contribute to the global inhibition of translation during starvation. It is currently unclear as to how phosphorylation of eIF6 modulates its association with the 60S maturation complex and ribosome quality control complex.

Interestingly, partial loss of eIF6 in *eIF6+/-* mice leads to increased accumulation of empty 80S complexes and smaller polysome peaks in the basal state[17-19]. This abrogates the stimulation of protein synthesis in response to insulin and growth factors[17-19]. The polysome profiles of *eIF6+/-* mice that were fasted overnight were similar to WT mice that showed enhanced accumulation of the empty 80S complex in response to fasting[19]. Since GSK3-activation during starvation is expected to inhibit eIF6, it is likely that the partial loss of eIF6 in the *eIF6+/-* mimics a starved basal state that leads to an accumulation of the empty 80S complex. Intriguingly, when the *eIF6+/-* mice were fed after overnight fasting, they were unable to stimulate protein synthesis in response to re-feeding, unlike the WT mice[19]. This suggests that eIF6 is critical for modulating protein synthesis during starvation, and activation of eIF6 may be critical for recovery from starvation. It is likely that eIF6 serves as an anti-association factor subsequent to the action of the eukaryotic ribosome recycling complexes[23,62]. Future studies will determine the precise contribution of GSK3-dependent phosphorylation of eIF6 towards ribosome biogenesis and 60S/40S association.

Acknowledgements

We thank Dr. Grzegorz Sabat and Dr. Greg Barrett-Wilt at the University of Wisconsin-Madison Mass Spectrometry Core for helping us generate the mass spectrometry data. We also thank Dr. Edwin Antony for his intellectual input and for providing initial resources for the work. This study is supported by the NIH-R15GM119103 grant provided to CP. This study is supported by the NIH-GM126477 grant, by the Wisconsin Women's Health Foundation through the Markos

Family Breast Cancer Woman Faculty Scholar grant, and start-up funds provided by Marquette University to SO.

Author contributions

The study was conceived by SO, who designed and performed some of the preliminary experiments and critically analyzed the results generated by CJ, JE and DM, and wrote the manuscript. CJ performed most of the experiments, interpreted the results and generated the associated images. CJ, JE, and DM wrote the methods section of the manuscript, which was edited by SO. CP generated the GSK3 constructs and contributed to the design of the priming site mutant experiments and critically reviewed the manuscript. DM performed the immunofluorescence experiments and analyzed the data. Majority of the clones were generated by JE, who designed some of the molecular cloning strategies and analyzed the data.

Conflict of interest

The authors declare that they have no conflict of interest.

Figure Legends

Figure 1. GSK3β phosphorylates a multisite motif in the C-terminal tail of eIF6

A. Sequence alignment of the last 41 amino acid residues (205 to 245) in the C-terminal tail of human eIF6 (NP_001254739) with *Xenopus* (NP_001083080.1), mouse (NP_034709.1), and rat eIF6 (NP_001032429). The conserved residues are marked with an astrix. Putative GSK3-specific phospho sites and priming site in multisite motif-1 are indicated in pink (S212, S216, S220) and in multisite motif-2 are indicated in red (T231, S235, S239, S243).

B. HCT116 cells were transfected with myc-eIF6 or myc-empty vector, and 24 hours later, cells were briefly serum-starved in 0.1% FBS for 4 hours. For the *in vitro* kinase assay, myc-eIF6 or myc-vector controls were immunoprecipitated and incubated in the presence or absence of recombinant GSK3. *In vitro* kinase reactions were then subjected to autoradiography and western blotting using anti-eIF6 antibody. Each experiment was repeated three independent times. Asterisks indicate the presence of a doublet as seen by autoradiography and western blotting.

C. The deletion mutant lacking both motif-1 and motif-2 (eIF6-CΔ36) was generated by substitution of T210. Myc-eIF6-FL or myc-eIF6-CΔ36 were transfected into HCT116 cells, and the *in vitro* kinase reactions were carried out as described above (Fig. 1B), except that the

western blot was probed with anti-myc antibody instead of the anti-eIF6 monoclonal antibody. Anti-eIF6 antibody (Cell Signaling Technology) is targeted to the C-terminal tail of eIF6 and does not recognize the eIF6-CΔ36 mutant. Each experiment was repeated three independent times. Asterisks indicate the presence of a doublet as seen by autoradiography and western blotting.

D. Mass Spectral (MS) analysis was carried out on myc-eIF6 immunoprecipitated from serum-starved HCT116 cells that were incubated with or without recombinant GSK3. Samples were excised from coomassie-stained acrylamide gels and analyzed by *nano*LC-MS/MS analysis. Plot shows the MS/MS spectrum along with matched fragmentation mass table showing specific T231 phosphorylation in the region of interest.

Figure 2. GSK3β phosphorylates multiple sites of eIF6 in a sequence

A. The deletion mutant lacking just motif-2 (eIF6-CΔ20) was generated by substitution of E226 with a stop codon. Myc-eIF6-FL or myc-eIF6-CΔ20 was immunoprecipitated from serum-starved HCT116 cells, and the *in vitro* kinase reactions were assayed by autoradiography and western blotting. Each experiment was repeated three independent times.

B. For the eIF6-3A and eIF6-4A mutants, the specific phospho-sites that were substituted with alanines are indicated and compared to the sequence of eIF6-FL.

C and D. Myc-eIF6-FL or myc-tagged phospho-site mutants were immunoprecipitated from HCT116 cells that were serum-starved in 0.1% FBS for 4 hours. *In vitro* kinase reactions were carried out in the presence and absence of recombinant GSK3β and were analyzed by autoradiography and by western blotting using anti-myc antibody. Each experiment was repeated three independent times.

E. For *nano*LC-MS/MS analysis, an eIF6 phosphopeptide (23 amino acids) carrying a phosphate at S243, the putative priming site, was synthesized (Aapptec) and incubated with recombinant GSK3β. Extracted ion chromatograms show relative abundance levels of singly (pre-charged) and multiple residues phosphorylated by GSK3β in the region of interest.

Figure 3. Priming dependent phosphorylation of eIF6 by GSK3β

A. GST-GSK3β-WT, GST-GKS3β-R96A mutant, or myc-eIF6 were transfected into 293T cells and 24 hours later, cells were briefly serum-starved in 0.1% FBS for 4 hours. GST-GSK3β-WT

or GST-GKS3β-R96A was pulled-down and eluted with glutathione as described in methods. Myc-eIF6 was immunoprecipitated from 293T cells. GST-GSK3β-WT or GST-GKS3β-R96A was incubated in the presence and absence of myc-eIF6 for the *in vitro* kinase reactions. Kinase reactions were screened by autoradiography and by western blotting. Blots were probed with anti-eIF6 and anti-GST antibodies. Each experiment was repeated three independent times. Asterisks indicate the presence of a doublet as seen by autoradiography and western blotting.

B and C. To capture interactions between GST-GKS3β and endogenous eIF6, HCT116 cells were transfected with GST-GKS3β or empty vector. 24 hours later, cells were serum starved in 0.1% FBS for 4 hours. GST-GKS3β, empty vector, or empty-vector lysate incubated with recombinant GST were pulled-down and any associated endogenous eIF6 (indicated by arrow) was detected by western blotting (**B**). Blots were probed with anti-GKS3β, anti-eIF6 and anti-GST antibodies. Whole-cell lysates (inputs) of samples used for the pull-downs in Fig. 3B were analyzed by western blotting and probed with the indicated antibodies (**C**). β-Actin was used as the loading control. Each experiment was repeated three independent times.

D. Lysates of HCT116 cells were collected just prior to starvation at 0 hours and again at 4, 8, and 18hour time points. Samples were analyzed by western blotting and blots were probed with anti-eIF6 antibody and anti-αTubulin antibody (loading control) (n=3).

E. Total eIF6 protein levels were quantitated using the blots represented in **D**. Values represent the standard error of the mean (SEM) of three independent experiments. Comparison of each time point with the 0 hour time point was not found to be significant as determined by one-way ANOVA (Dunnett's multiple comparison test).

Figure 4. Altered subcellular localization of eIF6 in response to serum-starvation is regulated by GSK3.

A. HCT116 cells were serum starved in 0.1% FBS for 24 hours, and were treated for a short-term (3 hours) with either vehicle (0.1% DMSO), 10μM CHIR99021or 25μM SB415286. Cells fed with 10% FBS and treated with vehicle were used as the non-starved controls. Cells were fixed and stained for endogenous eIF6 (red) using anti-eIF6 monoclonal antibody (Cell Signaling Technology) and nuclei were stained with DAPI (blue) and analyzed by immunofluorescence microscopy. Each experiment was repeated three independent times. Scale bar =100μm.

B. For nuclear and cytoplasmic extraction, HCT116 cells were serum-fed (lanes 1, 2) or serum starved in 0.1% FBS for 24 hours (lanes 3, 4) followed by subcellular fractionation. Samples were analyzed by western blotting. Blots were probed with anti-eIF6, anti-αTubulin (cytoplasmic marker), and anti-Topoisomerase IIβ antibodies (nuclear marker). Each experiment was repeated four independent times.

C. For inhibitor analysis, HCT116 cells were serum starved in 0.1% FBS for 24 hours and treated for a short-term (5 hours) with vehicle (lanes 1, 2) or 10μM CHIR99021 (lanes 3, 4) followed by subcellular fractionation. Samples were analyzed by western blotting and blots were probed with anti-eIF6, anti-αTubulin, and anti-Topoisomerase IIβ antibodies. Each experiment was repeated three independent times.

Figure 5. GSK3 regulates the starvation-dependent subcellular localization of eIF6 in normal cells

A. Normal RIE-1 cells were serum starved in 0.1% FBS for 24 hours and treated for a short-term (4 hours) with either vehicle or 10μM CHIR99021. Cells fed with 10% FBS and treated with vehicle were used as the non-starved controls. Cells were fixed and stained for endogenous eIF6 (red) and nuclei were stained with DAPI (blue) (n=3), and analyzed by immunofluorescence microscopy. Scale bar =100μm.

B. Proposed model for regulation of eIF6 by GSK3

In response to starvation or in the absence of nutrients or growth factor stimulation, GSK3 is potently activated by the inhibition of AKT and mTOR signaling pathways. Active GSK3 phosphorylates eIF6 on three specific sites, which is potentiated by priming at the C-terminal site by an unidentified kinase. eIF6 exhibits cytoplasmic accumulation in response to stress induced by serum-starvation. Phosphorylation of eIF6 by GSK3 is important for its cytoplasmic retention in response to starvation. It is unclear if cytoplasmic retention of eIF6 disrupts its nucleolar functions and contributes to an inhibition of 60S biogenesis in response to starvation. Since S235 is one of the sites of phosphorylation, we propose that GSK3-dependent phosphorylation of eIF6 at S235, T231, and S239 prevents its association with the 60S subunit. This could lead to an increase in empty 80S formation in response to starvation, which could contribute to the attenuation of global protein synthesis in concert with other adaptive mechanisms such as an inhibition of mTOR, and GSK3-dependent inhibition of eIF2B.

Supplementary Figure Legends

Figure S1. Activation of GSK3 in response to serum starvation

A. HCT116 cells were serum-starved for 18 hours in 0.1% FBS. Cell lysates were collected just prior to serum-starvation at 0 hours and at the time points indicated. Samples were analyzed by western blotting and blots were probed with anti-GSK3 (total), anti-GSK3-pS9 or anti-Vinculin antibody (loading control) (n=3).

B. GSK3-Serine-9 phosphorylation levels were quantitated using the blots represented in Fig. S1A. Values represent the SEM of three independent experiments. Asterisks indicate significantly different as determined by a one-way ANOVA (Dunnett's multiple comparison test). The difference in eIF6 levels between 0 hour versus 4 hours was not significant, 0 hour versus 8 hours was significant with p=0.0008, and 0 hour versus 18 hours was significant with p=0.0001.

Figure S2. Identification of eIF6-T231 phosphorylation by MS/MS analysis

A. MS analysis of the peptide was carried out as described in Fig. 1D. Extracted Ion Chromatograms for the indicated unphosphorylated peptide signal is normalized to the highest.

B. Mass spectrum of the indicated peptide shows normalized values averaged across extracted chromatogram.

C. Extracted Ion Chromatograms for the indicated phosphorylated peptide are represented with signal normalized to the highest.

D. Mass spectrum of the phosphorylated 'peptide of interest' with normalization to the highest values averaged across extracted chromatogram.

Figure S3. Quantitation of phosphorylation levels of the phospho-site mutants of eIF6

A. HCT116 cells were transfected with myc-eIF6-FL or myc-empty vector and subjected to immunoprecipitation followed by *in vitro* kinase reactions in the presence and absence of recombinant GSK3β as described previously (Fig. 1C). Asterisk indicates the presence of a non-specific band observed for the myc-vector control (lane 1) after prolonged exposure (4 days). Each experiment was repeated three independent times.

B. Graph represents the fold change in the phosphorylated levels of the eIF6-S243A phospho-site mutant relative to the eIF6-FL as determined from the autoradiographs indicated in Fig. 2C.

Values represent the SEM of three independent experiments. Asterisks indicate significantly different as determined by an unpaired two-tailed t-Test: $p<0.0001$.

C. Graph represents the fold change in the phosphorylated levels of the eIF6-T231A phospho-site mutant relative to the eIF6-FL as determined from the autoradiographs indicated in Fig. 2D. Values represent the SEM of three independent experiments. Asterisks indicate significantly different as determined by an unpaired two-tailed t-Test: $p=0.0201$.

D. MS analysis of the synthetic phosphopeptide was carried out as indicated in Fig. 2E. Extracted Ion Chromatograms and mass spectrum show multiple versions of the synthetic peptide and the relative abundance of the indicated synthetic peptides post *in vitro* phosphorylation.

Figure S4. Validation of altered subcellular localization of eIF6

A. HCT116 cells were fed with 10% FBS (non-starved controls) or starved in 0.1% FBS for 24 hours. Cells were fixed and stained for endogenous eIF6 (red) using anti-eIF6 monoclonal antibody (Santa Cruz Biotechnology) and nuclei were stained with DAPI (blue) and analyzed by immunofluorescence microscopy (n=3). Scale bar = 250μm.

B. HCT116 cells were serum-starved in 0.1% FBS for 24 hours and treated for a short-term (3 hours) with either vehicle (0.1% DMSO) (lane 1), or 10μM CHIR99021 (lane 2), or 25μM SB415286 (lane 3). Whole cell lysates were then analyzed by western blotting using anti-β-Catenin-phospho-S33/S37/T41 antibody and anti-αTubulin antibody (loading control) (n=3).

C. Blots represented in B. were quantitated and values represent the SEM of three independent experiments. Percent change in β-Catenin-phospho-S33/S37/T41 levels relative to the vehicle control was plotted. The differences were found to be significant as determined by an unpaired two-tailed t-Test with $p=0.0023$ for CHIR99021 versus vehicle and $p=0.0029$ for SB415286 versus vehicle.

Figure S5. Quantitation of nuclear-cytoplasmic levels of eIF6

A. Whole cell lysates of samples subjected to nuclear-cytoplasmic fractionation in Fig. 4B were assayed for total levels of eIF6, αTubulin and Topoisomerase IIβ by western blotting (n=4).

B. Whole cell lysates of samples subjected to nuclear-cytoplasmic fractionation in Fig. 4C. were assayed for total levels of eIF6, αTubulin and Topoisomerase IIβ by western blotting (n=3).

C and D. Blots represented in Fig. 4B, were quantitated and values represent the SEM of four independent experiments. Percent of nuclear and cytoplasmic fractions relative to the total (sum of nuclear and cytoplasmic eIF6 levels) are plotted. Difference in eIF6 levels between the nuclear and cytoplasmic fractions for non-starved controls were not significant as determined by an unpaired two-tailed t-Test but were found to be significant for the starved sample and asterisks indicate: p=0.0015.

E and F. Blots represented in Fig. 4C were quantitated and values represent the SEM of three independent experiments. Percent of nuclear and cytoplasmic fractions relative to the total (sum of nuclear and cytoplasmic eIF6 levels) are plotted. The difference in eIF6 levels between the nuclear and cytoplasmic fractions for the starved-vehicle control was found to be significant as determined by an unpaired two-tailed t-Test and asterisk indicates: p=0.015, but no significant difference was found between the CHIR99021-treated fractions.

Materials and Methods

Cell Culture and Transfections

HCT116 cells (human colorectal carcinoma line) (America Type Culture Collection - ATCC) were maintained in McCoy's 5A medium supplemented with 10% fetal bovine serum (FBS), and 100U/mL penicillin and 100µg/mL streptomycin (Gibco). HEK293T/17 cells (a derivative of human embryonic kidney cells) (ATCC) were maintained in Dulbecco's Modified Eagle Medium supplemented with 10% FBS, and 100U/mL penicillin and 100µg/mL streptomycin (Gibco). For transfections, about 2 X 10^6 HCT116 and 2.5 X 10^6 293T cells were plated per 60 mm dish. Each dish was transfected with 4µg of plasmid DNA and 20µL of lipofectamine 2000 (Invitrogen). 24 hours later, cells were washed twice in phosphate buffered saline (PBS), and serum starved for 4 hours using respective media with 0.1% FBS only. 4 hours later, cells were washed twice in PBS and collected in mammalian cell lysis buffer (MCLB) (50mM Tris-Cl pH 8.0, 5mM ethylenediaminetetraacetic acid (EDTA), 0.5% IGEPAL, 150mM sodium chloride) that was supplemented with the following inhibitors just before lysis: 1mM phenylmethylsufonyl fluoride (PMSF), 1mM sodium fluoride, 10mM β-glycerophosphate, 1mM sodium vanadate, 2mM Dithiothreitol (DTT), 1X protease inhibitor cocktail (Sigma Aldrich), 1X phosphatase inhibitor cocktail (Santa Cruz Biotechnology). Lysates were rocked for 15 minutes at 4°C, followed by centrifugation at 14,000 rpm for 10 minutes at 4°C.

Plasmid Constructions

To clone human eIF6, mRNA was extracted from MCF7 (ATCC) cells using RNAaqueous Total RNA Isolation kit (Invitrogen) and cDNA was synthesized using the Superscript First Strand cDNA synthesis kit (Invitrogen). Using polymerase chain reaction (PCR), eIF6 ORF was cloned into the pCMV-myc plasmid (Clontech) using the respective forward and reverse primers carrying EcoRI and XhoI restriction sites:
5'-TATAAGAATTCTAATGGCGGTCCGAGCTTCGTTCGAGAAC-3',
5'-TATAACTCGAGTCAGGTGAGGCTGTCAATGAGGGAATC-3. GST-tagged GSK3β constructs were cloned into the pDEST™27 vector (ThermoFisher Scientific) as described previously[63]. All the pCMV-myc-eIF6 phospho-site mutants were generated using the Q5® Site-Directed Mutagenesis Kit (New England Biolabs) using the forward and reverse primers listed in Table 1. All plasmid constructs used in this study were verified by Sanger sequencing (Genewiz).

Immunoprecipitation

For immunoprecipitation of myc-eIF6, or myc-empty vector (Fig. 1B), lysates with 1.2mg of total protein were suspended in a final volume of 500µL of MCLB buffer supplemented with inhibitors. Lysates were pre-cleared with 20µL of protein A/G plus-conjugated agarose beads (Santa Cruz Biotechnology) and 1µL of normal mouse IgG (Santa Cruz Biotechnology). Protein A/G plus-agarose beads were washed in MCLB buffer before use. For pre-clearing, lysates were rotated for 20 minutes at 4°C. Pre-cleared lysates were collected by centrifugation at 3500 rpm for 3 minutes at 4°C, and the beads were discarded. For immunoprecipitation, pre-cleared samples were incubated with 20µL of protein A/G plus-agarose beads and 11µL of myc-tag antibody (9E10) (Santa Cruz Biotechnology) and rotated overnight at 4°C. Samples were washed three times in MCLB buffer and the beads were collected by centrifugation at 3000 rpm for 3 minutes and washed for a fourth time in incomplete kinase (IK) buffer (50mM Tris, pH7.4, 10mM $MgCl_2$, 2mM DTT), and after the final wash, beads were suspended in 45µL of IK buffer. Immunoprecipitation of the myc-tagged phospho-site mutants of eIF6, eIF6-CΔ20, and myc-eIF6-FL was carried out as described above except that 1.5mg of total protein was used for the assay. For the myc-eIF6-CΔ36 mutant, owing to a small reduction in its expression, 2mg of total

protein was used for the assay. This ensured that the total eIF6 protein input for the kinase assays were comparable between eIF6-FL and the eIF6-CΔ36 mutant.

***In vitro* kinase assay**

For the *in vitro* kinase assays, myc-tagged versions of eIF6 were immunoprecipitated as indicated above and the immunoprecipitated beads were incubated with, or without 350 units of recombinant GSK3β (rabbit skeletal muscle) (New England BioLabs) and 1X hot kinase buffer (50mM Tris, pH 7.4, 50mM $MgCl_2$, 10mM DTT, 50μM cold ATP, γ-^{32}P-ATP- 1μCi), and incubated at 30°C for 30 minutes. Kinase reactions were also set-up for the analysis of phospho-site mutants of eIF6 and eIF6-FL control as detailed above except that the reactions were incubated at 30°C for 25 minutes to account for time-dependent kinetic differences. Kinase reactions were analyzed by SDS-PAGE and exposed to X-ray film for autoradiography. For western blotting of the kinase assay, duplicate kinase reactions were simultaneously set-up as described above except that the reactions were set-up using the cold kinase buffer (50mM Tris, pH 7.4, 50mM $MgCl_2$, 10mM DTT, 250μM cold ATP). Blots were probed with anti-eIF6 monoclonal antibody (1:1000), or anti-myc-tag monoclonal antibody (1:750), and anti-GSK3β monoclonal antibody (1:1000) (Cell Signaling Technology) diluted in Tris-buffered saline with 0.1% Tween-20 (TBS-T).

Pull-down assay

To determine interactions with the endogenous eIF6, HCT116 cells were transfected with GST-GSK3β or empty vector as previously described. Cell lysis was carried out in MCLB buffer as described above and a small fraction was saved for analysis of input levels. For the pull-down assays, 1.1mg of total protein suspended in 500μL of MCLB buffer and supplemented with inhibitors, was incubated with 50μL of glutathione agarose resin beads (Gold Biotechnology) and rotated overnight at 4°C. To determine interactions with the GST-only control, recombinant GST was purified from BL21 Codon-Plus *E. coli* using glutathione affinity chromatography, and 500ng of recombinant GST was incubated with lysates transfected with the empty vector control at 4°C. Next day, samples were washed three times in MCLB buffer supplemented with inhibitors and resuspended in (30μL) of MCLB buffer and 2X Laemmli buffer. Samples were then analyzed by western blotting. For the pull-down of GST-GSK3β-wild type and GST-

GSK3β-R96A, 293T cells were transfected with the respective vectors and 1.9mg of total protein was used for the pull-down analysis. Pull-downs were carried out as described above except that the active kinase was eluted from the glutathione agarose beads using glutathione (10mM reduced glutathione in 50mM Tris-HCl, pH 8.0). For the kinase assay, fresh eluates were incubated with myc-eIF6 that was immunoprecipitated (2mg total protein) from 293T cells.

Western blotting

For western blotting, proteins were resolved by SDS-polyacrylamide gel electrophoresis (SDS/PAGE). For all blots, about 20-40μg of total protein was loaded per lane, except for the kinase reactions where samples were prepared as described above. Proteins were transferred onto nitrocellulose membranes (0.45 micron, Bio-Rad Laboratories). Blots were blocked either for 1 hour or overnight in 5% non-fat dry milk diluted in TBS-T. The following primary antibodies dissolved in TBS-T were used: anti-GST antibody (1:1000, overnight), anti-αTubulin antibody (1:1000, overnight), anti-β-actin antibody (1:3000, 1hr), anti-eIF6 antibody (1:1000, overnight), anti-GSK3β antibody (1:1000, overnight) anti-phospho GSK3β (Ser-9) antibodies (1:1000, overnight), anti-myc-tag antibody (1:1000, overnight) (Cell Signaling Technology). To assay for GSK3β interaction with endogenous eIF6, blots were probed with anti-eIF6 monoclonal antibody (1:500) and incubated overnight (Cell Signaling Technology). To assay for β-catenin phosphorylation, 100μg of total protein was loaded per lane and blots were probed with anti-phospho-β-catenin (Ser33/37/Thr41) antibody (1:750 in 5% milk-TBS-T) and incubated overnight. Secondary antibodies (Jackson ImmunoResearch) were diluted 1:30000 in TBS-T. Blots were developed using ECL western blotting substrate (Pierce). For western blotting of nuclear and cytoplasmic fractions, 20μg of total protein was loaded per lane and probed with the following primary antibodies dissolved in TBS-T: Topoisomerase IIβ (1:1000, overnight) (BD Biosciences), αTubulin (DMIA) (1:3000, 1hr) and anti-eIF6 antibody (D1696) (1:1000, overnight) (Cell Signaling Technology).

Mass Spectrometry

For mass spectrometry, 7 X 10^6 293T cells were plated per 10cm plate and transfected as indicated before. 24 hours later, cells were serum-starved in DMEM containing 0.1% FBS for 3 hours. Cells were lysed in MCLB buffer supplemented with inhibitors. Immunoprecipitations

were carried out as previously described using 3mg of total protein. For the kinase reactions, 15µL of myc-eIF6-bound beads were incubated with/without recombinant GSK3β (NEB) and suspended in cold kinase buffer and incubated at 30°C for 30 minutes. Reactions were washed twice in incomplete kinase buffer, and resuspended in incomplete kinase buffer and 1.5X Laemmli buffer. Samples were boiled and analyzed by SDS-PAGE followed by Coomassie staining. Stained gels were sent to the University of Wisconsin-Madison Mass Spectrometry facility.

Enzymatic "In Gel" Digestion

"In gel" digestion and mass spectrometric analysis was done at the Mass Spectrometry Facility [Biotechnology Center, University of Wisconsin-Madison]. In short, Colloidal Coomassie G-250 stained gel pieces were de-stained twice for 5 minutes in MeOH:H_20:NH_4HCO_3 [50%:50%:100mM], dehydrated for 5 minutes in ACN:H_20:NH_4HCO_3 [50%:50%:25mM] then once more for 30 seconds in 100% ACN, dried in a Speed-Vac for 2minutes, rehydrated completely and reduced in 25mM DTT (in 25mM NH_4HCO_3) for 30 minutes at 56°C, alkylated by solution exchange with 55mM Iodoacetamide (in 25mM NH_4HCO_3) in the dark at room temperature for 30 minutes, washed once in 25mM NH_4HCO_3, dehydrated twice for 5 minutes in ACN:H_20:NH_4HCO_3 [50%:50%:25mM] then once more for 30 seconds in 100% ACN, dried in a Speed-Vac again and finally rehydrated with 20µL of trypsin solution [10ng/µL trypsin (PROMEGA) in 25mM NH_4HCO_3 and 0.01% ProteaseMAX w/v (PROMEGA)]. Additional 30µL of digestion solution [25mM NH_4HCO_3 and 0.01% ProteaseMAX w/v (PROMEGA)] was added to facilitate complete rehydration with excess overlay needed for peptide extraction. The digestion was conducted for 3 hours at 42°C. Peptides generated from digestion were transferred to a new tube and acidified with 2.5% Triflouroacetiacid (TFA) to 0.3% final concentration. Gel pieces were extracted further with ACN:H_2O:TFA [70%:29.25%:0.75%] for 10 minutes and solutions combined then dried completely in a Speed-Vac (~15 minutes). Extracted peptides were solubilized in 30µL of 0.1% formic acid and degraded in ProteaseMAX and removed via centrifugation [max speed, 10 minutes]. 10µL was taken for immediate solid phase extraction (ZipTip® C18 pipette tips Millipore) according to manufacturer protocol. Remaining 20µLwas subjected to a secondary digestion with endoproteinase AspN (Roche) where pH was adjusted with 2.5µL 500mM

NH_4HCO_3 and 1µL of 40ng/µL AspN stock added. Digestion was carried out for 2 hours at 37°C subsequently acidified with 2.5% TFA to 0.3% final and solid phase extracted as conventional tryptic digest. Peptides eluted off ZipTip C18 tips with ACN:H_2O:TFA [70%:29.9%:0.1%] were dried and finally solubilized in 8µL of 0.1% formic acid.

NanoLC-MS/MS

Peptides were analyzed by nano liquid chromatography tandem mass spectrometry using the Agilent 1100 nanoflow system (Agilent) connected to a hybrid linear ion trap-orbitrap mass spectrometer (LTQ-Orbitrap Elite™, Thermo Fisher Scientific) equipped with an EASY-Spray™ electrospray source. Chromatography of peptides prior to mass spectral analysis was accomplished using capillary emitter column (PepMap® C18, 3µM, 100Å, 150x0.075mm, Thermo Fisher Scientific) onto which 3µL of extracted peptides was automatically loaded. NanoHPLC system delivered solvents A: 0.1% (v/v) formic acid, and B: 99.9% (v/v) acetonitrile, 0.1% (v/v) formic acid at 0.50 µL/min to load the peptides (over a 30 minute period) and 0.3µl/min to elute peptides directly into the nano-electrospray with gradual gradient from 3% (v/v) B to 20% (v/v) B over 17 minutes and concluded with 5 minute fast gradient from 20% (v/v) B to 50% (v/v) B at which time a 4 minute flush-out from 50-95% (v/v) B took place. As peptides eluted from the HPLC-column/electrospray source survey MS scans were acquired in the Orbitrap with a resolution of 120,000 followed by MS2 fragmentation of 20 most intense peptides detected in the MS1 scan from 350 to 1800 m/z; redundancy was limited by dynamic exclusion.

Data analysis

Raw MS/MS data was converted to mgf file format using MSConvert (ProteoWizard: Open Source Software for Rapid Proteomics Tools Development). Resulting mgf files were used to search against Uniprot Human amino acid sequence database containing a list of common contaminants and decoy entries (134,183 total entries) using in-house *Mascot* search engine 2.2.07 (Matrix Science) with variable Serine and Threonine phosphorylation, Methionine oxidation, Asparagine and Glutamine deamidation plus fixed Cysteine carbamidomethylation. Peptide mass tolerance was set at 15 ppm and fragment mass at 0.6 Da.

Mass spectrometry of phosphopeptide

100µM of the synthesized phosphopeptide (Aapptec) was incubated with 350units of recombinant GSK3β (New England Biolabs) and cold kinase buffer. Reactions were incubated for 20 minutes at 30°C. Reactions were then quenched by 40mM EDTA and by freezing.

NanoLC-MS/MS

100µM of synthesized version of human eIF6 phosphopeptide was acidified with 2.5% TFA to 0.4% final and solid phase extracted (ZipTip C18 pipette tips, Millipore) according to manufacturer protocol. Peptide was eluted off ZipTip C18 tip with 2µl of ACN:H_2O:TFA [70%:29.9%:0.1%] and diluted to 20µL final volume with 0.1% formic acid. Mass spectrometric analysis followed using the Agilent 1100 nanoflow system (Agilent) connected to a hybrid linear ion trap-orbitrap mass spectrometer (LTQ-Orbitrap Elite™, Thermo Fisher Scientific) equipped with an EASY-Spray™ electrospray source. Chromatography of peptides prior to mass spectral analysis was accomplished using capillary emitter column (PepMap C18, 3µM, 100Å, 150x0.075mm, Thermo Fisher Scientific) onto which 2µL of extracted peptides was automatically loaded. NanoHPLC system delivered solvents A: 0.1% (v/v) formic acid , and B: 99.9% (v/v) acetonitrile, 0.1% (v/v) formic acid at 0.50 µL/min to load the peptides (over a 30 minute period) and 0.3µL/min to elute peptides directly into the nano-electrospray with gradual gradient from 3% (v/v) B to 20% (v/v) B over 17 minutes and concluded with 5 minute fast gradient from 20% (v/v) B to 50% (v/v) B at which time a 4 minute flush-out from 50-95% (v/v) B took place. As peptides eluted from the HPLC-column/electrospray source survey MS scans were acquired in the Orbitrap with a resolution of 120,000 followed by MS2 fragmentation of 20 most intense peptides detected in the MS1 scan from 350 to 1800 m/z; redundancy was limited by dynamic exclusion. Raw MS/MS data was converted to mgf file format using MS Convert (ProteoWizard: Open Source Software for Rapid Proteomics Tools Development). Resulting mgf files were used to search specifically against human eIF6 sequence using in-house *Mascot* search engine 2.2.07 (Matrix Science) with variable Serine and Threonine phosphorylation. Peptide mass tolerance was set at 15 ppm and fragment mass at 0.6 Da. Dynamic phosphorylation cascade distributions were manually interrogated for precursor ion abundance and quality of MS/MS fragmentation.

Immunofluorescence Staining and Microscopy

50,000 HCT116 cells were plated in each well of a 12-well plate carrying poly-D-lysine-coated glass coverslips (Neuvitro). After overnight incubation, cells were either serum-fed with McCoy's 5A medium containing 10% FBS or serum-starved in media containing 0.1% FBS, and 24 hours later, treated with either 0.1% dimethyl sulfoxide (DMSO) (vehicle), or 10μM CHIR99021 (Tocris), or 25μM SB415286 (Tocris). Cells were fixed overnight in 2% paraformaldehyde/PBS. For immunostaining, fixed cells were permeabilized with 2% Triton X-100/PBS for 20 minutes and incubated in blocking buffer (2% BSA/0.1% IGEPAL/PBS) for 30 minutes. The following primary antibodies diluted in the blocking buffer were used for staining: anti-eIF6 monoclonal antibody (D16E9) (1:300) (Cell Signaling Technology), or anti-eIF6 monoclonal antibody (1:350) (Santa Cruz Biotechnology) and incubated in a humidified chamber at room temperature (RT) for 1 hour. Coverslips were washed with 0.1% IGEPAL/PBS and incubated with Cy3-conjugated affinipure donkey anti-rabbit IgG secondary antibody (Jackson ImmunoResearch) diluted in blocking buffer (1:300) at RT for 1 hour in the dark. Coverslips were washed in 0.1% IGEPAL/PBS and mounted using ProLong Gold antifade reagent with 4'-6-Diamidino-2-phenylindole (DAPI) (Invitrogen). Staining of normal rat intestinal epithelial cells (RIE-1) was carried out as described above except that 30,000 cells were plated per well, and cells were probed with anti-eIF6 monoclonal antibody (D16E9) (1:200) (Cell Signaling Technology). RIE-1 cells were cultured and maintained as described previously[64,65]. For imaging, slides were analyzed using the Leica DM6 B upright fluorescent microscope. Images were acquired using Leica DFC 3000G (Bin 1x1, Gamma1) camera and processed by Leica LAS X imaging software.

Subcellular Fractionation

700,000 HCT116 cells were plated per 100mm dish and 24 hours later, cells were serum-starved in media containing 0.1% FBS or serum-fed with media containing 10% FBS for an additional 24 hours. To assay the effect of inhibitors, serum-starved cells were treated with either 0.1% DMSO (vehicle) or 10μM CHIR99021 (Tocris) for 5 hours. To assay for total protein input, cells were lysed in MCLB buffer supplemented with inhibitors as previously described. To extract cytoplasmic fractions, cells were collected in cell lysis buffer (10 mM HEPES, pH 7.5, 10 mM KCl, 0.1 mM EDTA, 0.5% IGEPAL) supplemented with the following inhibitors: 10mM β-

glycerophosphate, 1mM sodium vanadate, 2mM DTT, 1X protease inhibitor cocktail (Sigma Aldrich), 1X phosphatase inhibitor cocktail (Santa Cruz Biotechnology) and 0.5mM PMSF. Nuclear-cytoplasmic fractionation was carried out as described before[66]. For cytoplasmic fractionation, lysates were incubated on ice for 15 minutes with intermittent gentle mixing and vortexed for 10 seconds at 14000 rpm. Cells were centrifuged at 12,000 x g for 10 minutes at 4°C and cytoplasmic lysates were collected. For nuclear extraction, nuclear pellets were washed four times in cell lysis buffer at 3000 rpm for 5 minutes at 4°C. Nuclear pellets were suspended in 75µL of nuclear extract buffer (20mM HEPES, pH 7.5, 400mM sodium chloride, 1mM EDTA,) supplemented with the following inhibitors: 10mM β-glycerophosphate, 1mM sodium vanadate, 2mM DTT, 1X protease inhibitor cocktail (Sigma Aldrich), 1X phosphatase inhibitor cocktail (Santa Cruz Biotechnology) and 0.5mM PMSF. Nuclear pellets were solubilized on ice for 30 minutes followed by centrifugation at 12,000 x g for 15 minutes at 4°C. Both nuclear and cytoplasmic fractions were analyzed by western blotting.

Table 1. Primers used to generate phospho-site mutants of eIF6 by site-directed mutagenesis

Primer	**Sequence (5' to 3')**
eIF6-CΔ20-F	CAAGCTGAATTAAGCCCAGCCTA
eIF6-CΔ20-R	AAGACACTCTCCACCACTG
eIF6-S243A-F	CCTCATTGACGCCCTCACCTGACTCG
eIF6-S243A-R	GAATCCCGCATGCTGGTG
eIF6-CΔ36-F	TGGCCTGGACTGAACCAGCACA
eIF6-eIF6-CΔ36-R	CAGAAGGCACACCAGTCA
eIF6-4A-F	GGATGCCCTCATTGACGCCCTCACCTGACTCGAGGTAC
eIF6-4A-R	CGCATGGCGGTGGCAATGGCGCTAGGCTGGGCTTCATT
eIF6-T231A-F	CCAGCCTAGCGCCATTGCCACCA
eIF6-T231A-R	GCTTCATTCAGCTTGAAGACACTCTCC
eIF6-3A-F	CATGCGGGATGCCCTCATTGACAGCCTCACC
eIF6-3A-R	GCGGTGGCAATGGCGCTAGGCTGGGCTTCATT
eIF6-S235A-F	CATTGCCACCGCCATGCGGGATTCC
eIF6-S235A-R	GTGCTAGGCTGGGCTTCA
eIF6-S239A-F	CATGCGGGATGCCCTCATTGA
eIF6-S239A-R	CTGGTGGCAATGGTGCTA

References

1 Brina, D., Grosso, S., Miluzio, A. & Biffo, S. Translational control by 80S formation and 60S availability: the central role of eIF6, a rate limiting factor in cell cycle progression and tumorigenesis. *Cell Cycle* **10**, 3441-3446, doi:10.4161/cc.10.20.17796 (2011).

2 Brina, D., Miluzio, A., Ricciardi, S. & Biffo, S. eIF6 anti-association activity is required for ribosome biogenesis, translational control and tumor progression. *Biochim Biophys Acta* **1849**, 830-835, doi:10.1016/j.bbagrm.2014.09.010 (2015).

3 Miluzio, A., Beugnet, A., Volta, V. & Biffo, S. Eukaryotic initiation factor 6 mediates a continuum between 60S ribosome biogenesis and translation. *EMBO Rep* **10**, 459-465, doi:10.1038/embor.2009.70 (2009).

4 Malyutin, A. G., Musalgaonkar, S., Patchett, S., Frank, J. & Johnson, A. W. Nmd3 is a structural mimic of eIF5A, and activates the cpGTPase Lsg1 during 60S ribosome biogenesis. *EMBO J* **36**, 854-868, doi:10.15252/embj.201696012 (2017).

5 Ma, C. *et al.* Structural snapshot of cytoplasmic pre-60S ribosomal particles bound by Nmd3, Lsg1, Tif6 and Reh1. *Nat Struct Mol Biol* **24**, 214-220, doi:10.1038/nsmb.3364 (2017).

6 Kater, L. *et al.* Visualizing the Assembly Pathway of Nucleolar Pre-60S Ribosomes. *Cell* **171**, 1599-1610 e1514, doi:10.1016/j.cell.2017.11.039 (2017).

7 Basu, U., Si, K., Warner, J. R. & Maitra, U. The Saccharomyces cerevisiae TIF6 gene encoding translation initiation factor 6 is required for 60S ribosomal subunit biogenesis. *Mol Cell Biol* **21**, 1453-1462, doi:10.1128/MCB.21.5.1453-1462.2001 (2001).

8 Senger, B. *et al.* The nucle(ol)ar Tif6p and Efl1p are required for a late cytoplasmic step of ribosome synthesis. *Mol Cell* **8**, 1363-1373 (2001).

9 Russell, D. W. & Spremulli, L. L. Purification and characterization of a ribosome dissociation factor (eukaryotic initiation factor 6) from wheat germ. *J Biol Chem* **254**, 8796-8800 (1979).

10 Gartmann, M. *et al.* Mechanism of eIF6-mediated inhibition of ribosomal subunit joining. *J Biol Chem* **285**, 14848-14851, doi:10.1074/jbc.C109.096057 (2010).

11 Weis, F. *et al.* Mechanism of eIF6 release from the nascent 60S ribosomal subunit. *Nat Struct Mol Biol* **22**, 914-919, doi:10.1038/nsmb.3112 (2015).

12 Ceci, M. *et al.* Release of eIF6 (p27BBP) from the 60S subunit allows 80S ribosome assembly. *Nature* **426**, 579-584, doi:10.1038/nature02160 (2003).

13 Finch, A. J. *et al.* Uncoupling of GTP hydrolysis from eIF6 release on the ribosome causes Shwachman-Diamond syndrome. *Genes Dev* **25**, 917-929, doi:10.1101/gad.623011 (2011).

14 Pesce, E. *et al.* Direct and high throughput (HT) interactions on the ribosomal surface by iRIA. *Sci Rep* **5**, 15401, doi:10.1038/srep15401 (2015).

15 Klinge, S., Voigts-Hoffmann, F., Leibundgut, M., Arpagaus, S. & Ban, N. Crystal structure of the eukaryotic 60S ribosomal subunit in complex with initiation factor 6. *Science* **334**, 941-948, doi:10.1126/science.1211204 (2011).

16 Groft, C. M., Beckmann, R., Sali, A. & Burley, S. K. Crystal structures of ribosome anti-association factor IF6. *Nat Struct Biol* **7**, 1156-1164, doi:10.1038/82017 (2000).

17 Gandin, V. *et al.* Eukaryotic initiation factor 6 is rate-limiting in translation, growth and transformation. *Nature* **455**, 684-688, doi:10.1038/nature07267 (2008).

18 Miluzio, A. *et al.* Impairment of cytoplasmic eIF6 activity restricts lymphomagenesis and tumor progression without affecting normal growth. *Cancer Cell* **19**, 765-775, doi:10.1016/j.ccr.2011.04.018 (2011).

19 Brina, D. *et al.* eIF6 coordinates insulin sensitivity and lipid metabolism by coupling translation to transcription. *Nat Commun* **6**, 8261, doi:10.1038/ncomms9261 (2015).

20 Wong, C. C., Traynor, D., Basse, N., Kay, R. R. & Warren, A. J. Defective ribosome assembly in Shwachman-Diamond syndrome. *Blood* **118**, 4305-4312, doi:10.1182/blood-2011-06-353938 (2011).

21 Clarke, K. *et al.* The Role of Eif6 in Skeletal Muscle Homeostasis Revealed by Endurance Training Co-expression Networks. *Cell Rep* **21**, 1507-1520, doi:10.1016/j.celrep.2017.10.040 (2017).

22 Ashe, M. P., De Long, S. K. & Sachs, A. B. Glucose depletion rapidly inhibits translation initiation in yeast. *Mol Biol Cell* **11**, 833-848, doi:10.1091/mbc.11.3.833 (2000).

23 van den Elzen, A. M., Schuller, A., Green, R. & Seraphin, B. Dom34-Hbs1 mediated dissociation of inactive 80S ribosomes promotes restart of translation after stress. *EMBO J* **33**, 265-276, doi:10.1002/embj.201386123 (2014).

24 Liu, B. & Qian, S. B. Characterizing inactive ribosomes in translational profiling. *Translation (Austin)* **4**, e1138018, doi:10.1080/21690731.2015.1138018 (2016).

25 Jastrzebski, K., Hannan, K. M., Tchoubrieva, E. B., Hannan, R. D. & Pearson, R. B. Coordinate regulation of ribosome biogenesis and function by the ribosomal protein S6 kinase, a key mediator of mTOR function. *Growth Factors* **25**, 209-226, doi:10.1080/08977190701779101 (2007).

26 Iadevaia, V., Liu, R. & Proud, C. G. mTORC1 signaling controls multiple steps in ribosome biogenesis. *Semin Cell Dev Biol* **36**, 113-120, doi:10.1016/j.semcdb.2014.08.004 (2014).

27 Krokowski, D. *et al.* Characterization of hibernating ribosomes in mammalian cells. *Cell Cycle* **10**, 2691-2702, doi:10.4161/cc.10.16.16844 (2011).

28 Manning, B. D. Adaptation to starvation: translating a matter of life or death. *Cancer Cell* **23**, 713-715, doi:10.1016/j.ccr.2013.05.012 (2013).

29 Nielsen, P. J., Duncan, R. & McConkey, E. H. Phosphorylation of ribosomal protein S6. Relationship to protein synthesis in HeLa cells. *Eur J Biochem* **120**, 523-527 (1981).

30 Sonenberg, N. & Hinnebusch, A. G. Regulation of translation initiation in eukaryotes: mechanisms and biological targets. *Cell* **136**, 731-745, doi:10.1016/j.cell.2009.01.042 (2009).

31 Tzamarias, D., Roussou, I. & Thireos, G. Coupling of GCN4 mRNA translational activation with decreased rates of polypeptide chain initiation. *Cell* **57**, 947-954 (1989).

32 Miluzio, A. *et al.* Translational control by mTOR-independent routes: how eIF6 organizes metabolism. *Biochem Soc Trans* **44**, 1667-1673, doi:10.1042/BST20160179 (2016).

33 Mertins, P. *et al.* Proteogenomics connects somatic mutations to signalling in breast cancer. *Nature* **534**, 55-62, doi:10.1038/nature18003 (2016).

34 Beli, P. *et al.* Proteomic investigations reveal a role for RNA processing factor THRAP3 in the DNA damage response. *Mol Cell* **46**, 212-225, doi:10.1016/j.molcel.2012.01.026 (2012).

35 Kettenbach, A. N. *et al.* Quantitative phosphoproteomics identifies substrates and functional modules of Aurora and Polo-like kinase activities in mitotic cells. *Sci Signal* **4**, rs5, doi:10.1126/scisignal.2001497 (2011).

36 Olsen, J. V. *et al.* Quantitative phosphoproteomics reveals widespread full phosphorylation site occupancy during mitosis. *Sci Signal* **3**, ra3, doi:10.1126/scisignal.2000475 (2010).

37 Imami, K. *et al.* Temporal profiling of lapatinib-suppressed phosphorylation signals in EGFR/HER2 pathways. *Mol Cell Proteomics* **11**, 1741-1757, doi:10.1074/mcp.M112.019919 (2012).

38 Klammer, M. *et al.* Phosphosignature predicts dasatinib response in non-small cell lung cancer. *Mol Cell Proteomics* **11**, 651-668, doi:10.1074/mcp.M111.016410 (2012).

39 Miluzio, A. *et al.* Expression and activity of eIF6 trigger malignant pleural mesothelioma growth in vivo. *Oncotarget* **6**, 37471-37485, doi:10.18632/oncotarget.5462 (2015).

40 Beurel, E., Grieco, S. F. & Jope, R. S. Glycogen synthase kinase-3 (GSK3): regulation, actions, and diseases. *Pharmacol Ther* **148**, 114-131, doi:10.1016/j.pharmthera.2014.11.016 (2015).

41 Cohen, P. & Frame, S. The renaissance of GSK3. *Nat Rev Mol Cell Biol* **2**, 769-776, doi:10.1038/35096075 (2001).

42 Frame, S. & Cohen, P. GSK3 takes centre stage more than 20 years after its discovery. *Biochem J* **359**, 1-16 (2001).

43 Frame, S., Cohen, P. & Biondi, R. M. A common phosphate binding site explains the unique substrate specificity of GSK3 and its inactivation by phosphorylation. *Mol Cell* **7**, 1321-1327 (2001).

44 Sutherland, C., Leighton, I. A. & Cohen, P. Inactivation of glycogen synthase kinase-3 beta by phosphorylation: new kinase connections in insulin and growth-factor signalling. *Biochem J* **296 (Pt 1)**, 15-19 (1993).

45 Cross, D. A. *et al.* The inhibition of glycogen synthase kinase-3 by insulin or insulin-like growth factor 1 in the rat skeletal muscle cell line L6 is blocked by wortmannin, but not by rapamycin: evidence that wortmannin blocks activation of the mitogen-activated protein kinase pathway in L6 cells between Ras and Raf. *Biochem J* **303 (Pt 1)**, 21-26 (1994).

46 Cross, D. A., Alessi, D. R., Cohen, P., Andjelkovich, M. & Hemmings, B. A. Inhibition of glycogen synthase kinase-3 by insulin mediated by protein kinase B. *Nature* **378**, 785-789, doi:10.1038/378785a0 (1995).

47 Proud, C. G. Regulation of eukaryotic initiation factor eIF2B. *Prog Mol Subcell Biol* **26**, 95-114 (2001).

48 Wang, X., Janmaat, M., Beugnet, A., Paulin, F. E. & Proud, C. G. Evidence that the dephosphorylation of Ser(535) in the epsilon-subunit of eukaryotic initiation factor (eIF) 2B is insufficient for the activation of eIF2B by insulin. *Biochem J* **367**, 475-481, doi:10.1042/BJ20020677 (2002).

49 Welsh, G. I., Miller, C. M., Loughlin, A. J., Price, N. T. & Proud, C. G. Regulation of eukaryotic initiation factor eIF2B: glycogen synthase kinase-3 phosphorylates a conserved serine which undergoes dephosphorylation in response to insulin. *FEBS Lett* **421**, 125-130 (1998).

50 Dajani, R. *et al.* Crystal structure of glycogen synthase kinase 3 beta: structural basis for phosphate-primed substrate specificity and autoinhibition. *Cell* **105**, 721-732 (2001).

51 ter Haar, E. *et al.* Structure of GSK3beta reveals a primed phosphorylation mechanism. *Nat Struct Biol* **8**, 593-596, doi:10.1038/89624 (2001).

52 Sutherland, C. What Are the bona fide GSK3 Substrates? *Int J Alzheimers Dis* **2011**, 505607, doi:10.4061/2011/505607 (2011).

53 Peifer, M., Pai, L. M. & Casey, M. Phosphorylation of the Drosophila adherens junction protein Armadillo: roles for wingless signal and zeste-white 3 kinase. *Dev Biol* **166**, 543-556, doi:10.1006/dbio.1994.1336 (1994).

54 Yost, C. *et al.* The axis-inducing activity, stability, and subcellular distribution of beta-catenin is regulated in Xenopus embryos by glycogen synthase kinase 3. *Genes Dev* **10**, 1443-1454 (1996).

55 Liu, C. *et al.* Control of beta-catenin phosphorylation/degradation by a dual-kinase mechanism. *Cell* **108**, 837-847 (2002).

56 Roach, P. J., Depaoli-Roach, A. A., Hurley, T. D. & Tagliabracci, V. S. Glycogen and its metabolism: some new developments and old themes. *Biochem J* **441**, 763-787, doi:10.1042/BJ20111416 (2012).

57 Roach, P. J. Control of glycogen synthase by hierarchal protein phosphorylation. *FASEB J* **4**, 2961-2968 (1990).

58 Coghlan, M. P. *et al.* Selective small molecule inhibitors of glycogen synthase kinase-3 modulate glycogen metabolism and gene transcription. *Chem Biol* **7**, 793-803 (2000).

59 Kramer, T., Schmidt, B. & Lo Monte, F. Small-Molecule Inhibitors of GSK-3: Structural Insights and Their Application to Alzheimer's Disease Models. *Int J Alzheimers Dis* **2012**, 381029, doi:10.1155/2012/381029 (2012).

60 Hagen, T., Di Daniel, E., Culbert, A. A. & Reith, A. D. Expression and characterization of GSK-3 mutants and their effect on beta-catenin phosphorylation in intact cells. *J Biol Chem* **277**, 23330-23335, doi:10.1074/jbc.M201364200 (2002).

61 Biswas, A. *et al.* Opposing action of casein kinase 1 and calcineurin in nucleo-cytoplasmic shuttling of mammalian translation initiation factor eIF6. *J Biol Chem* **286**, 3129-3138, doi:10.1074/jbc.M110.188565 (2011).

62 Pisareva, V. P., Skabkin, M. A., Hellen, C. U., Pestova, T. V. & Pisarev, A. V. Dissociation by Pelota, Hbs1 and ABCE1 of mammalian vacant 80S ribosomes and stalled elongation complexes. *EMBO J* **30**, 1804-1817, doi:10.1038/emboj.2011.93 (2011).

63 Zeidner, L. C., Buescher, J. L. & Phiel, C. J. A novel interaction between Glycogen Synthase Kinase-3alpha (GSK-3alpha) and the scaffold protein Receptor for Activated C-Kinase 1 (RACK1) regulates the circadian clock. *Int J Biochem Mol Biol* **2**, 318-327 (2011).

64 Origanti, S. & Shantz, L. M. Ras transformation of RIE-1 cells activates cap-independent translation of ornithine decarboxylase: regulation by the Raf/MEK/ERK and phosphatidylinositol 3-kinase pathways. *Cancer Res* **67**, 4834-4842, doi:10.1158/0008-5472.CAN-06-4627 (2007).

65 Origanti, S. *et al.* Ornithine decarboxylase mRNA is stabilized in an mTORC1-dependent manner in Ras-transformed cells. *Biochem J* **442**, 199-207, doi:10.1042/BJ20111464 (2012).

66 Schreiber, E., Matthias, P., Muller, M. M. & Schaffner, W. Rapid detection of octamer binding proteins with 'mini-extracts', prepared from a small number of cells. *Nucleic Acids Res* **17**, 6419 (1989).

Figure 1.

A

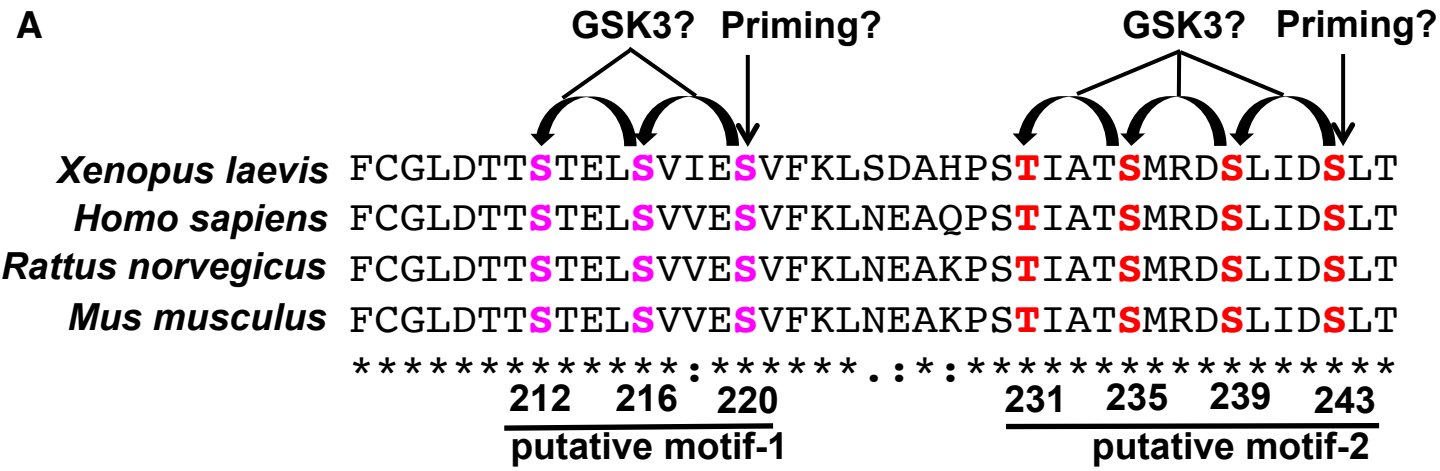

B

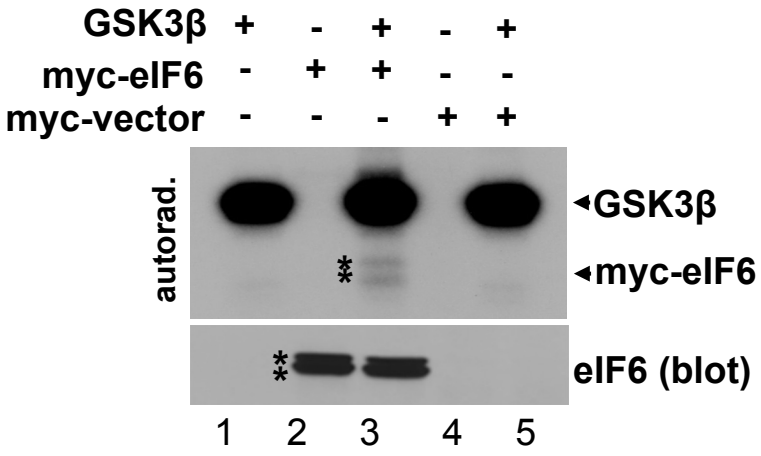

C

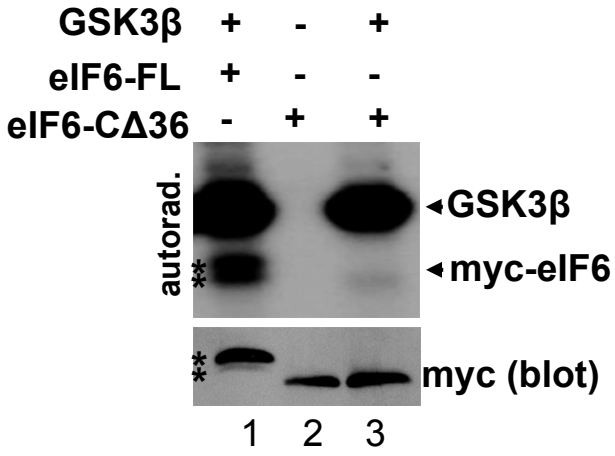

D

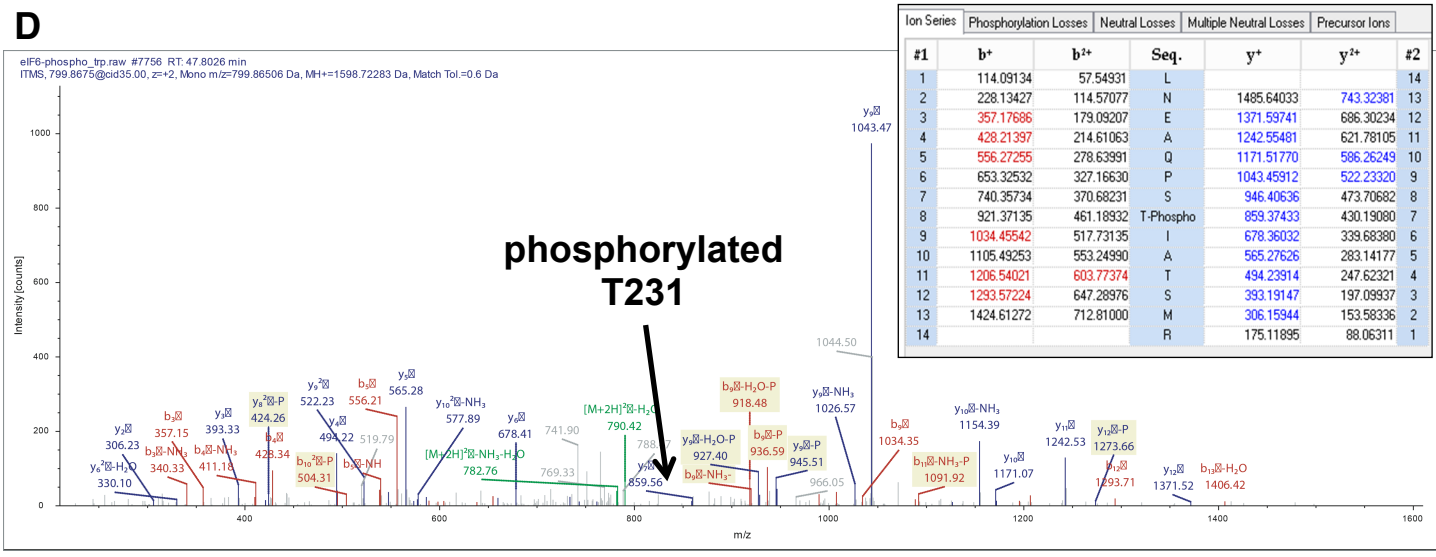

Ion Series	Phosphorylation Losses	Neutral Losses	Multiple Neutral Losses	Precursor Ions

#1	b+	b2+	Seq.	y+	y2+	#2
1	114.09134	57.54931	L			14
2	228.13427	114.57077	N	1485.64033	743.32381	13
3	357.17686	179.09207	E	1371.59741	686.30234	12
4	428.21397	214.61063	A	1242.55481	621.78105	11
5	556.27255	278.63991	Q	1171.51770	586.26249	10
6	653.32532	327.16630	P	1043.45912	522.23320	9
7	740.35734	370.68231	S	946.40636	473.70682	8
8	921.37135	461.18932	T-Phospho	859.37433	430.19080	7
9	1034.45542	517.73135	I	678.36032	339.68380	6
10	1105.49253	553.24990	A	565.27626	283.14177	5
11	1206.54021	603.77374	T	494.23914	247.62321	4
12	1293.57224	647.28976	S	393.19147	197.09937	3
13	1424.61272	712.81000	M	306.15944	153.58336	2
14			R	175.11895	88.06311	1

Figure 2.

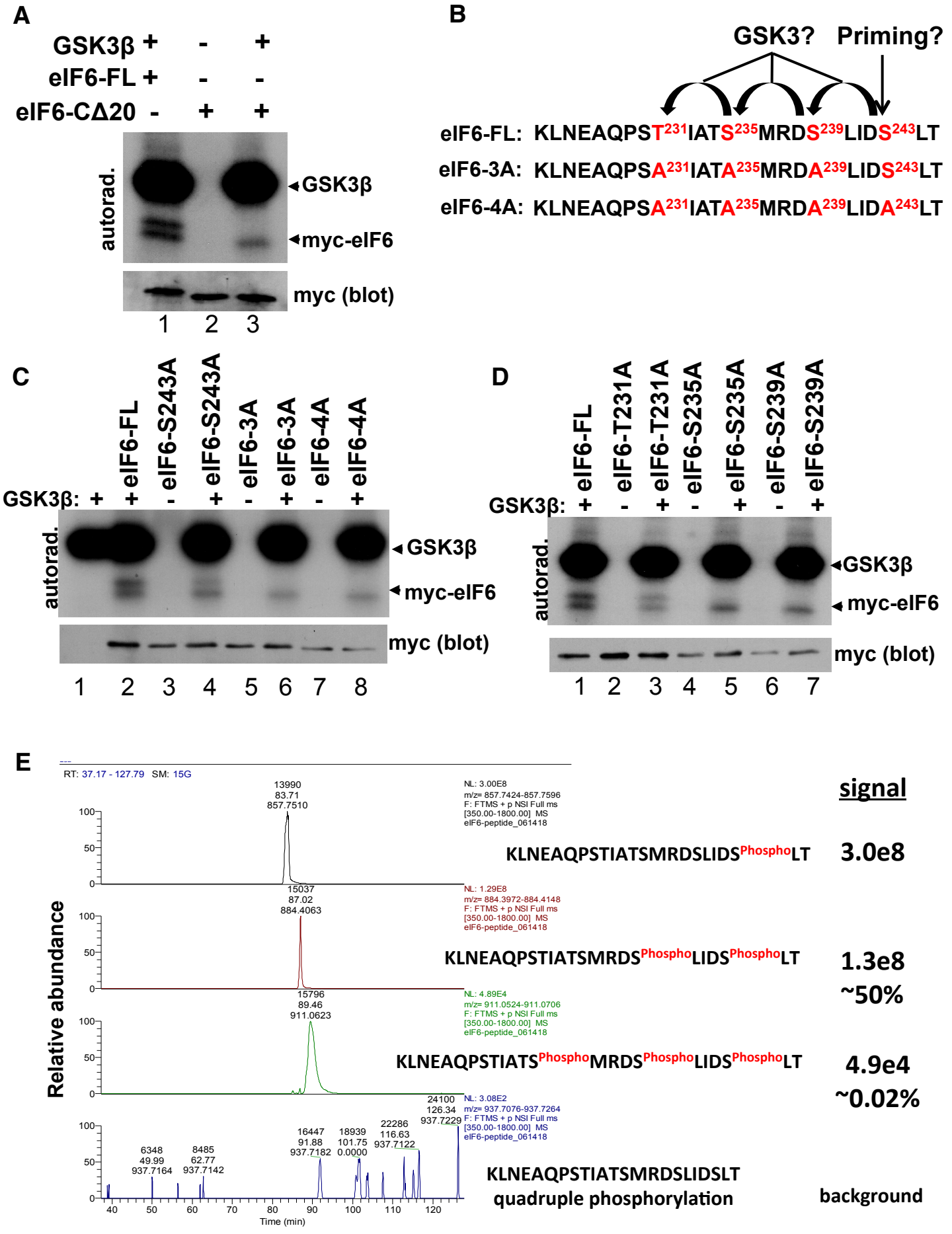
A
GSK3β + - +
eIF6-FL + - -
eIF6-CΔ20 - + +
autorad.
GSK3β
myc-eIF6
myc (blot)
1 2 3
B
GSK3? Priming?
eIF6-FL: KLNEAQPST231IATS235MRDS239LIDS243LT
eIF6-3A: KLNEAQPSA231IATA235MRDA239LIDS243LT
eIF6-4A: KLNEAQPSA231IATA235MRDA239LIDA243LT
C
GSK3β: + + eIF6-FL - eIF6-S243A + eIF6-S243A - eIF6-3A + eIF6-3A - eIF6-4A + eIF6-4A
autorad.
GSK3β
myc-eIF6
myc (blot)
1 2 3 4 5 6 7 8
D
GSK3β: + eIF6-FL - eIF6-T231A + eIF6-T231A - eIF6-S235A + eIF6-S235A - eIF6-S239A + eIF6-S239A
autorad.
GSK3β
myc-eIF6
myc (blot)
1 2 3 4 5 6 7
E
RT: 37.17 - 127.79 SM: 15G
13990
83.71
857.7510
NL: 3.00E8
m/z= 857.7424-857.7596
F: FTMS + p NSI Full ms
[350.00-1800.00] MS
eIF6-peptide_061418
KLNEAQPSTIATSMRDSLIDSPhosphoLT
signal
3.0e8
15037
87.02
884.4063
NL: 1.29E8
m/z= 884.3972-884.4148
F: FTMS + p NSI Full ms
[350.00-1800.00] MS
eIF6-peptide_061418
KLNEAQPSTIATSMRDSPhosphoLIDSPhosphoLT
1.3e8
~50%
15796
89.46
911.0623
NL: 4.89E4
m/z= 911.0524-911.0706
F: FTMS + p NSI Full ms
[350.00-1800.00] MS
eIF6-peptide_061418
KLNEAQPSTIATSPhosphoMRDSPhosphoLIDSPhosphoLT
4.9e4
~0.02%
24100
126.34
937.7229
NL: 3.08E2
m/z= 937.7076-937.7264
F: FTMS + p NSI Full ms
[350.00-1800.00] MS
eIF6-peptide_061418
6348
49.99
937.7164
8485
62.77
937.7142
16447
91.88
937.7182
18939
101.75
0.0000
22286
116.63
937.7122
KLNEAQPSTIATSMRDSLIDSLT
quadruple phosphorylation
background
Relative abundance
Time (min)

Figure 3.

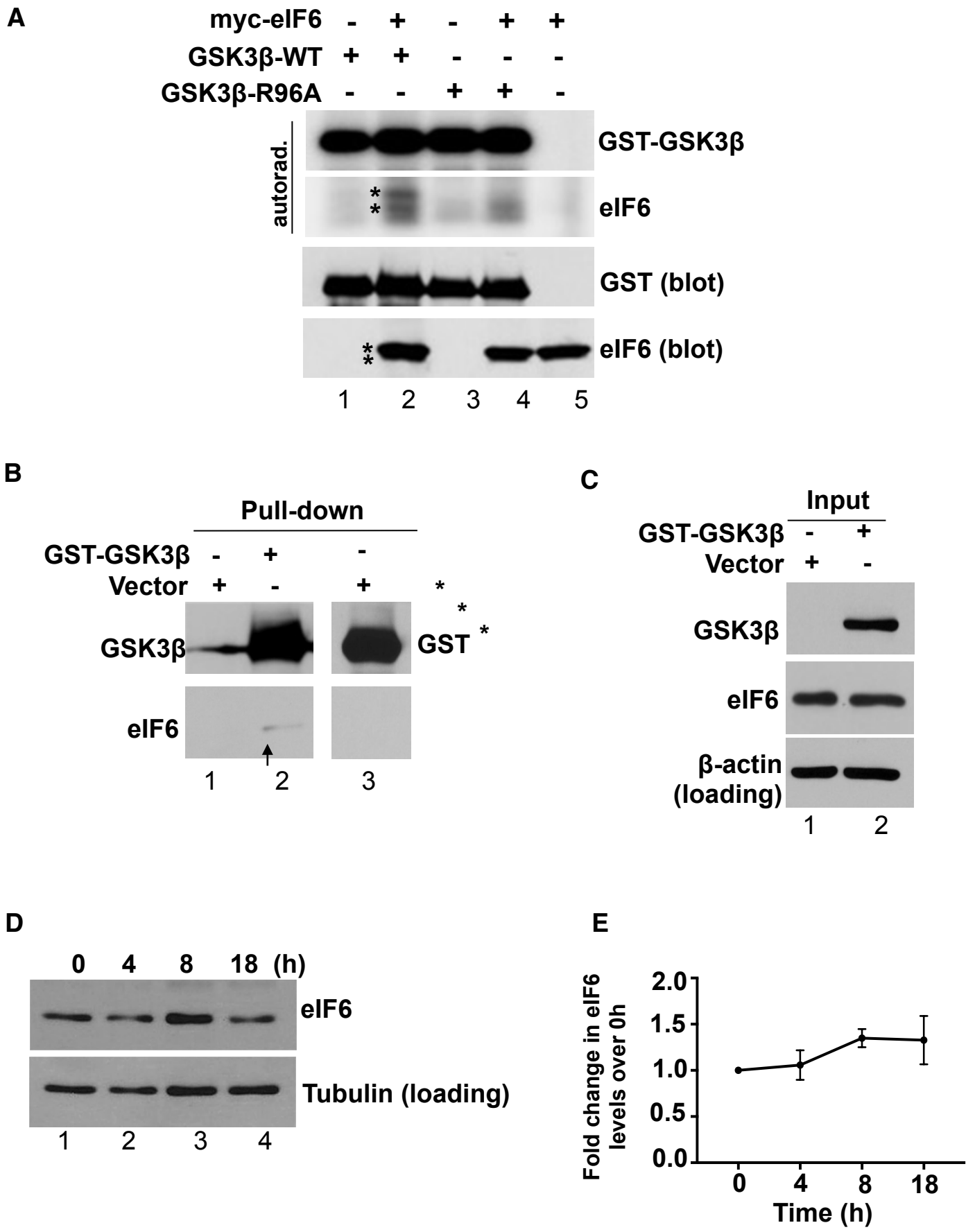
A
myc-eIF6 - + - + +
GSK3β-WT + + - - -
GSK3β-R96A - - + + -
autorad.
GST-GSK3β
eIF6
GST (blot)
eIF6 (blot)
1 2 3 4 5
B
Pull-down
GST-GSK3β - + -
Vector + - +
GSK3β
GST
eIF6
1 2 3
C
Input
GST-GSK3β - +
Vector + -
GSK3β
eIF6
β-actin (loading)
1 2
D
0 4 8 18 (h)
eIF6
Tubulin (loading)
1 2 3 4
E
Fold change in eIF6 levels over 0h
2.0
1.5
1.0
0.5
0.0
0 4 8 18
Time (h)

Figure 4.

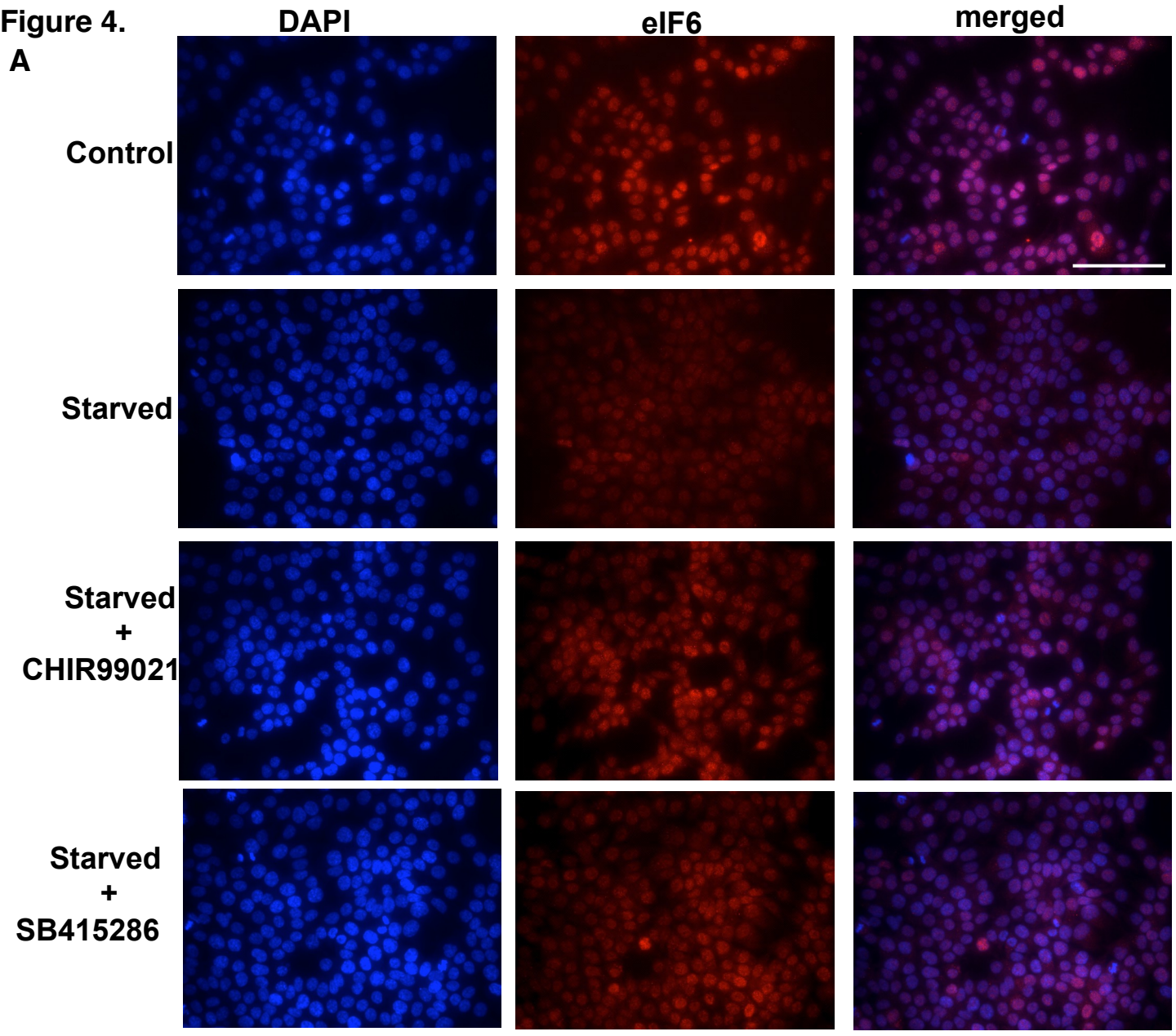
A
DAPI
eIF6
merged
Control
Starved
Starved
+
CHIR99021
Starved
+
SB415286

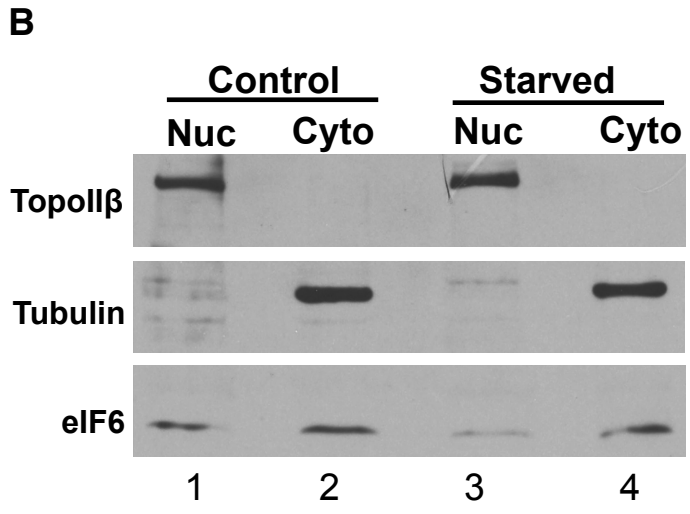
B
Control
Starved
Nuc
Cyto
Nuc
Cyto
TopoIIβ
Tubulin
eIF6
1
2
3
4

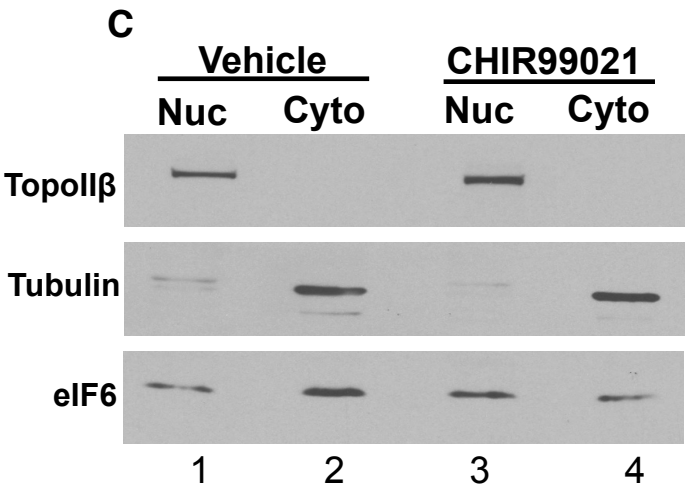
C
Vehicle
CHIR99021
Nuc
Cyto
Nuc
Cyto
TopoIIβ
Tubulin
eIF6
1
2
3
4

Figure 5.

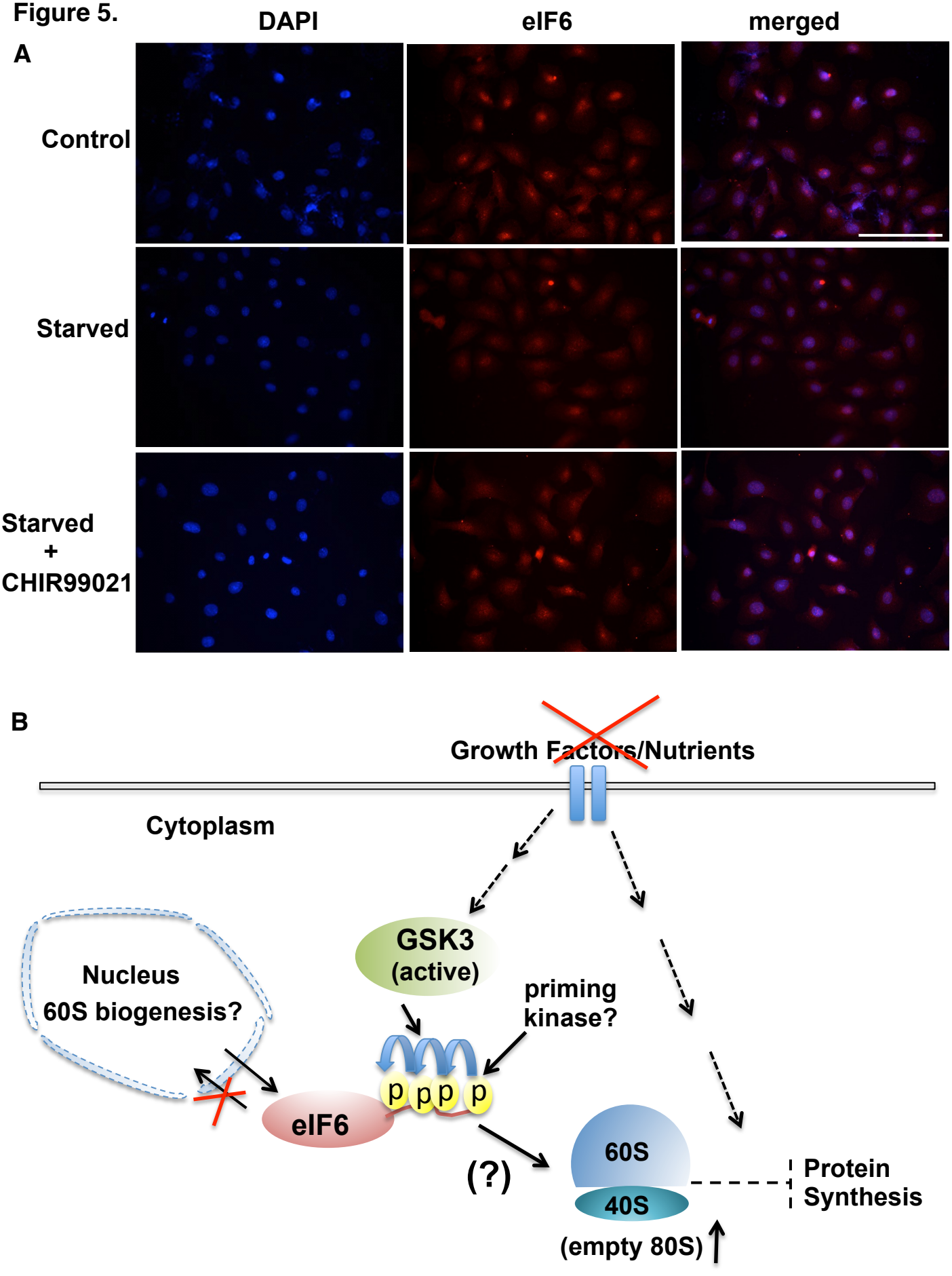
DAPI
eIF6
merged
A
Control
Starved
Starved
+
CHIR99021
B
Growth Factors/Nutrients
Cytoplasm
Nucleus
60S biogenesis?
GSK3
(active)
priming
kinase?
p p p p
eIF6
(?)
60S
40S
(empty 80S)
Protein
Synthesis

Figure S1.

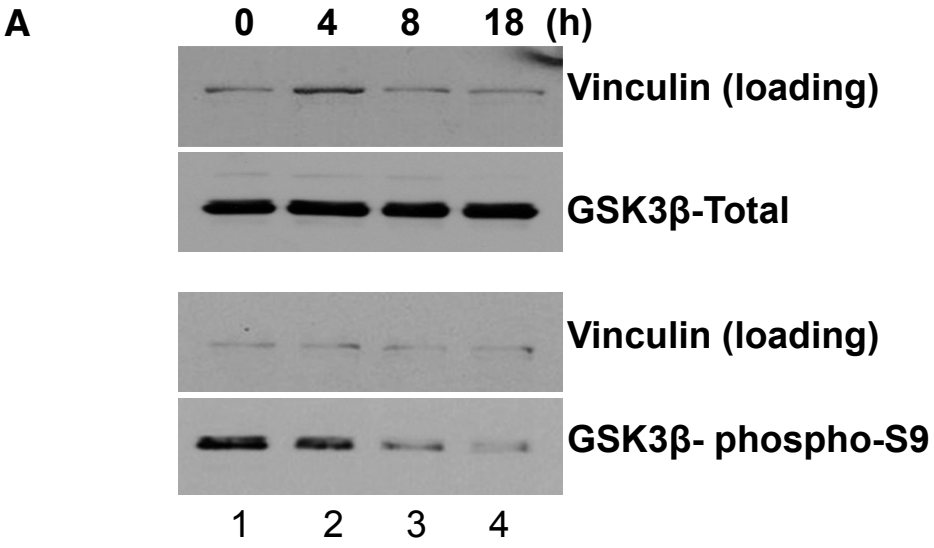
A
0
4
8
18
(h)
Vinculin (loading)
GSK3β-Total
Vinculin (loading)
GSK3β- phospho-S9
1
2
3
4

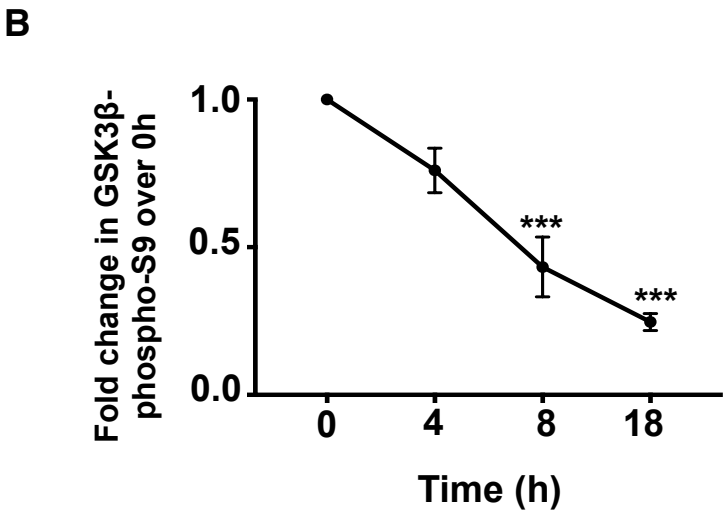
B
Fold change in GSK3β-phospho-S9 over 0h
1.0
0.5
0.0
***
***
0
4
8
18
Time (h)

Figure S2.

A

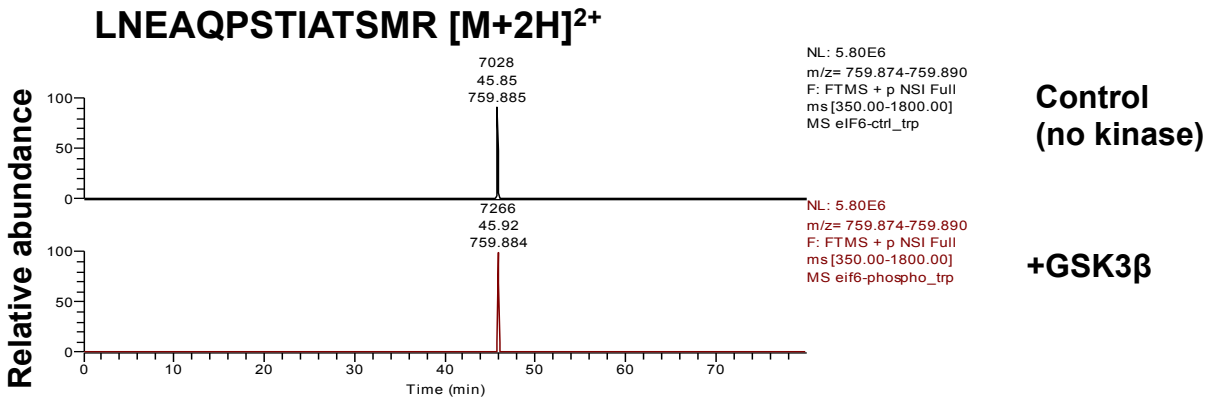

B

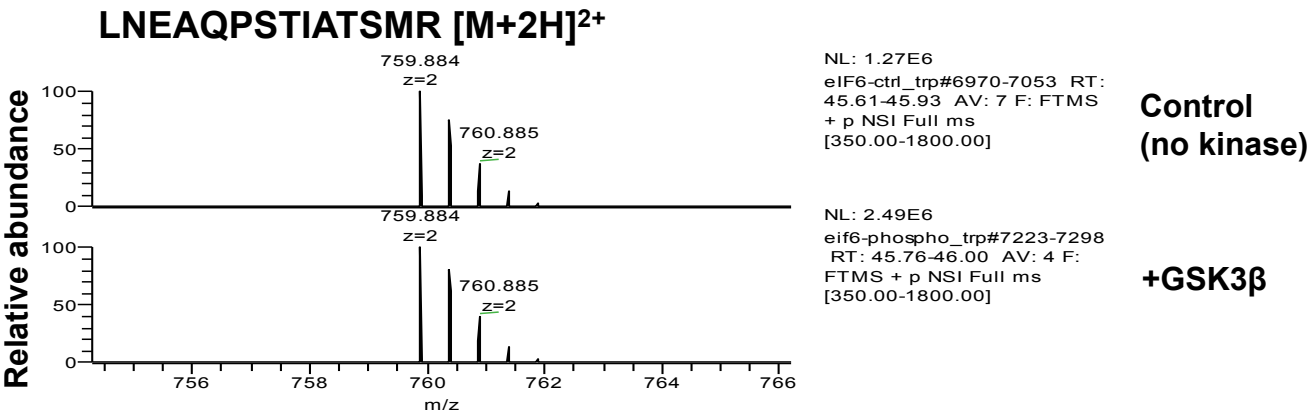

C

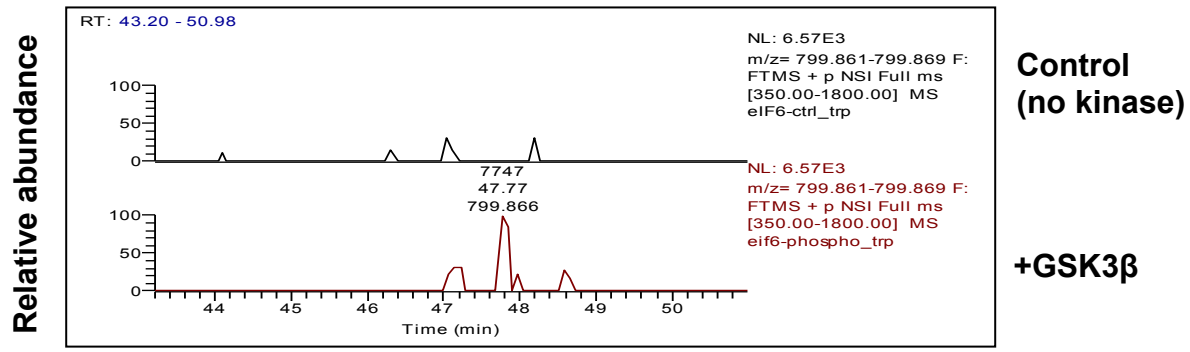

D

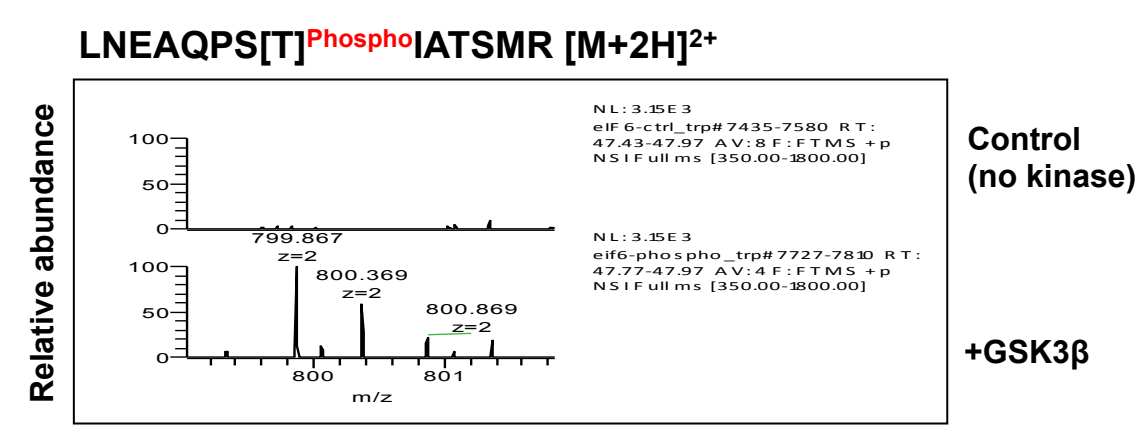

Figure S3.

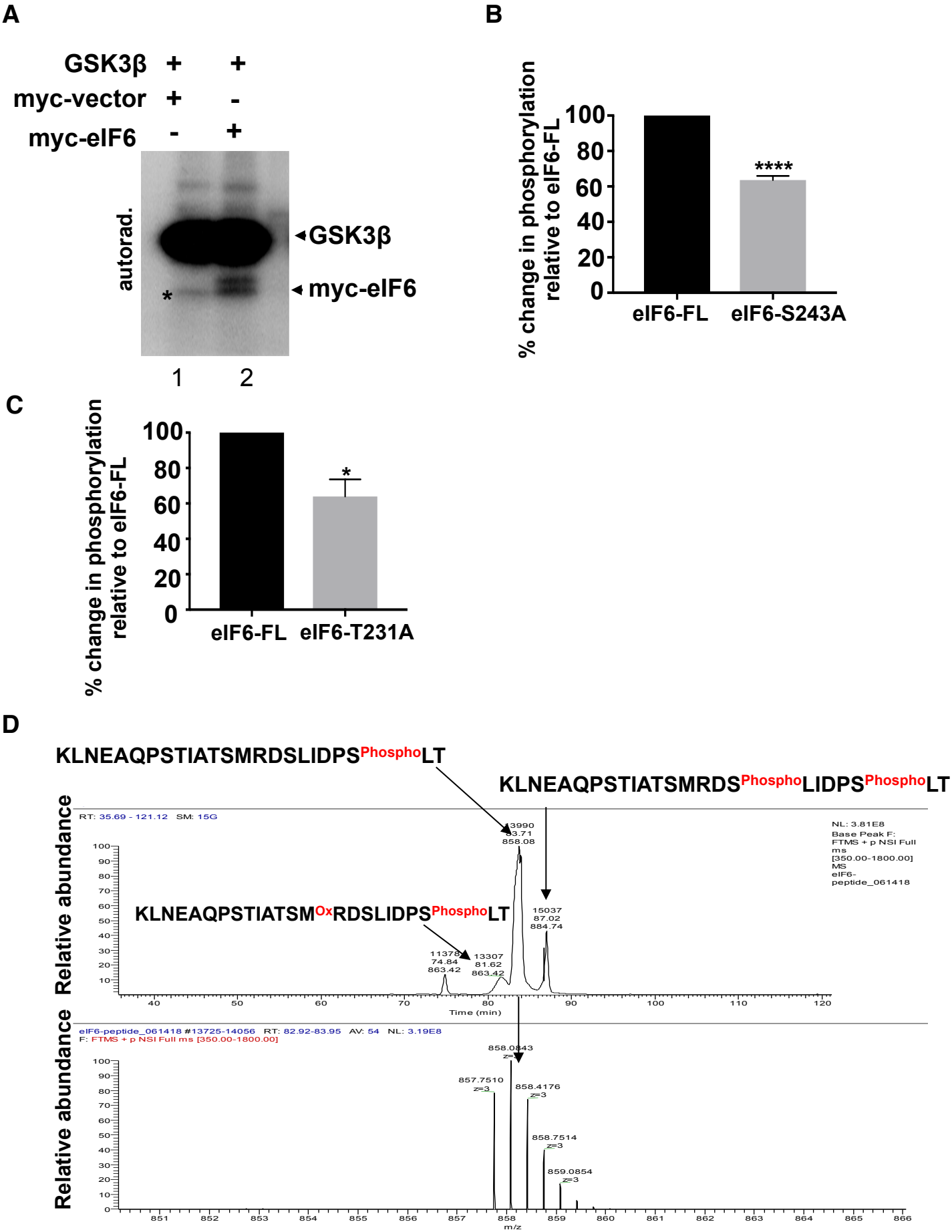
A
GSK3β + +
myc-vector + -
myc-eIF6 - +
autorad.
GSK3β
myc-eIF6
*
1 2
B
% change in phosphorylation relative to eIF6-FL
100
80
60
40
20
0
****
eIF6-FL
eIF6-S243A
C
% change in phosphorylation relative to eIF6-FL
100
80
60
40
20
0
*
eIF6-FL
eIF6-T231A
D
KLNEAQPSTIATSMRDSLIDPSPhosphoLT
KLNEAQPSTIATSMRDSPhosphoLIDPSPhosphoLT
KLNEAQPSTIATSMOxRDSLIDPSPhosphoLT
RT: 35.69 - 121.12 SM: 15G
NL: 3.81E8
Base Peak F: FTMS + p NSI Full ms [350.00-1800.00] MS eIF6-peptide_061418
13990 83.71 858.08
15037 87.02 884.74
11378 74.84 863.42
13307 81.62 863.42
Relative abundance
Time (min)
eIF6-peptide_061418 #13725-14056 RT: 82.92-83.95 AV: 54 NL: 3.19E8
F: FTMS + p NSI Full ms [350.00-1800.00]
858.0843 z=3
857.7510 z=3
858.4176 z=3
858.7514 z=3
859.0854 z=3
Relative abundance
m/z

Figure S4.

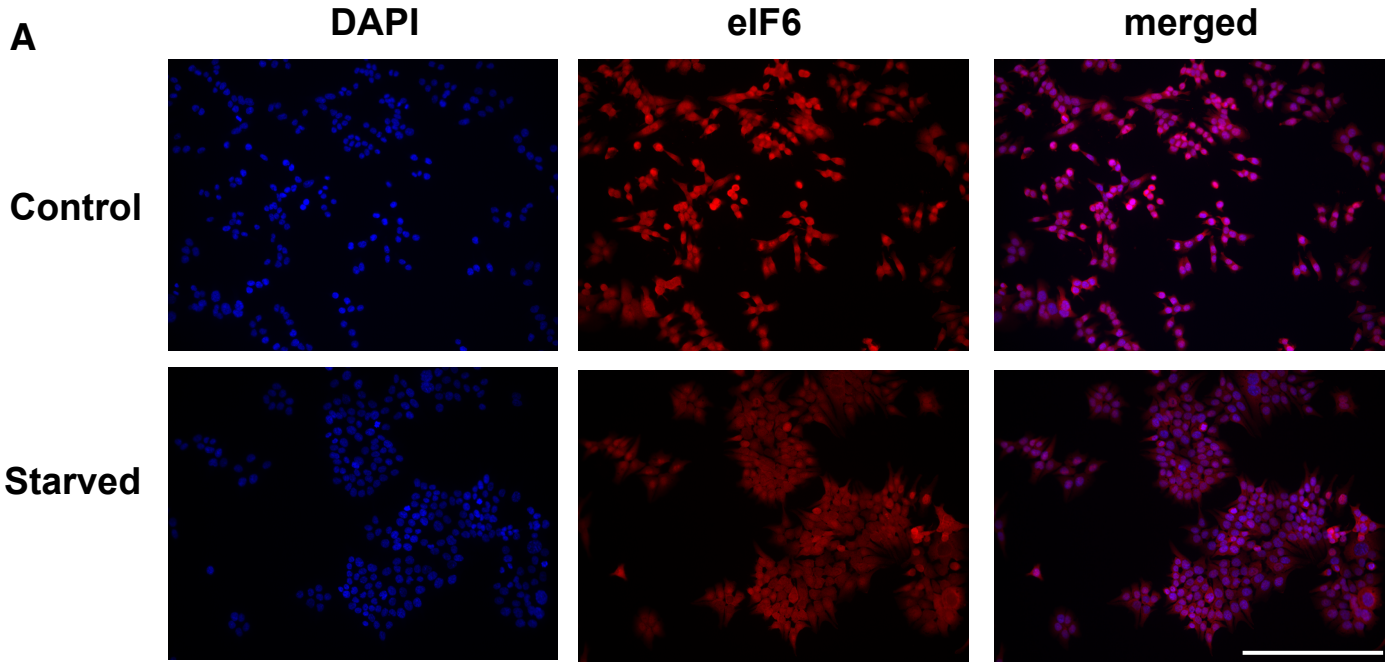
A
DAPI
eIF6
merged
Control
Starved

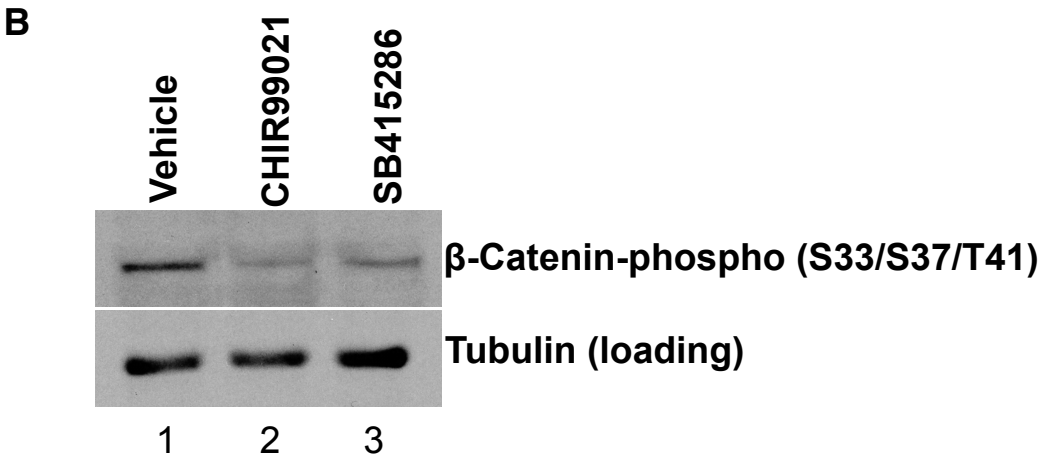
B
Vehicle
CHIR99021
SB415286
β-Catenin-phospho (S33/S37/T41)
Tubulin (loading)
1
2
3

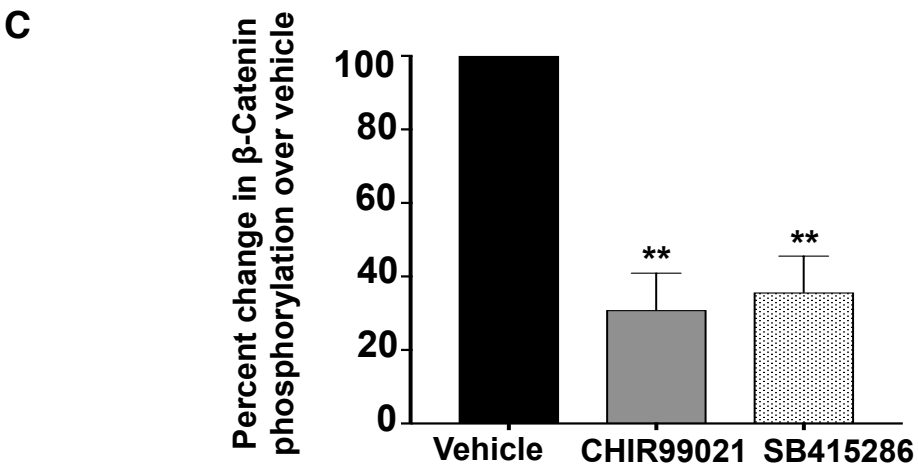
C
Percent change in β-Catenin phosphorylation over vehicle
100
80
60
40
20
0
**
**
Vehicle
CHIR99021
SB415286

Figure S5.

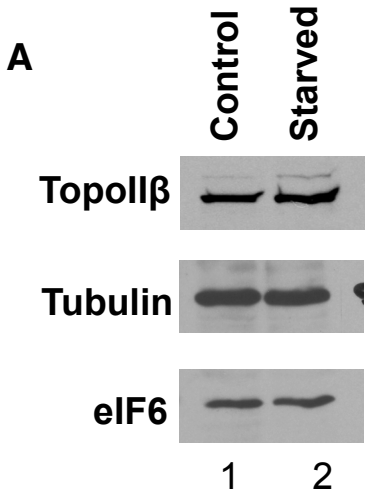
A
Control
Starved
TopoIIβ
Tubulin
eIF6
1
2

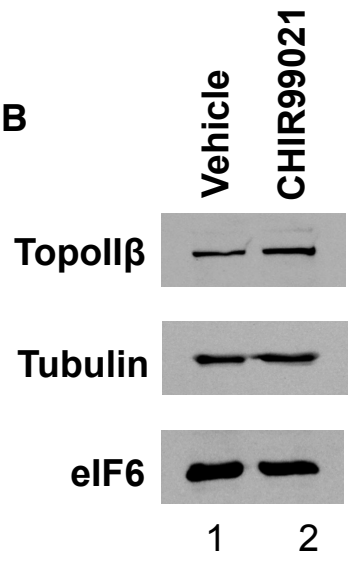
B
Vehicle
CHIR99021
TopoIIβ
Tubulin
eIF6
1
2

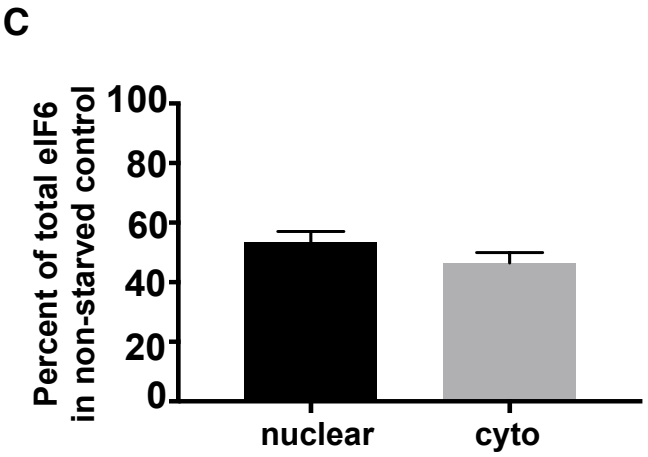
C
Percent of total eIF6 in non-starved control
100
80
60
40
20
0
nuclear
cyto

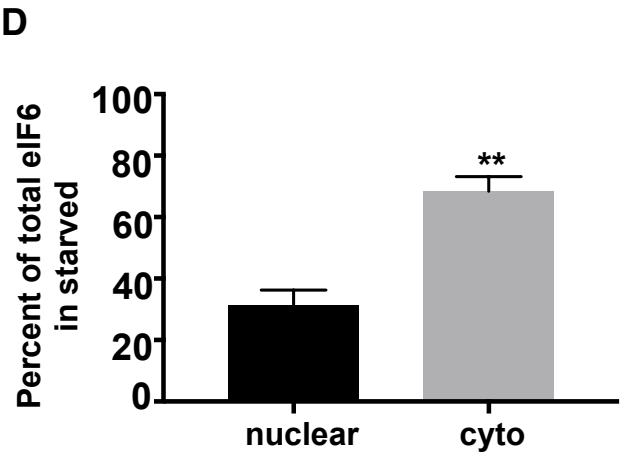
D
Percent of total eIF6 in starved
100
80
60
40
20
0
**
nuclear
cyto

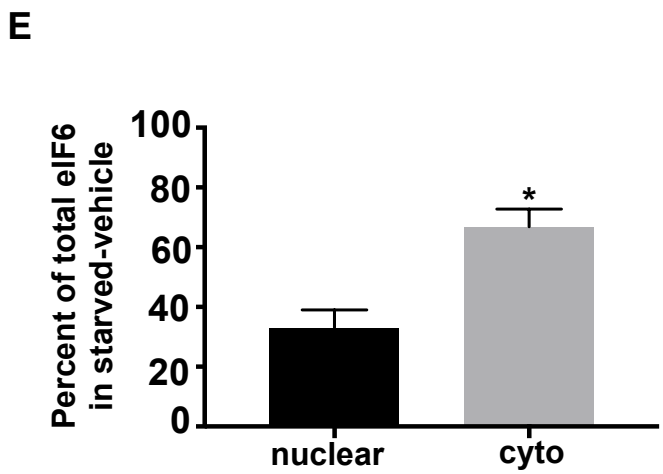
E
Percent of total eIF6 in starved-vehicle
100
80
60
40
20
0
*
nuclear
cyto

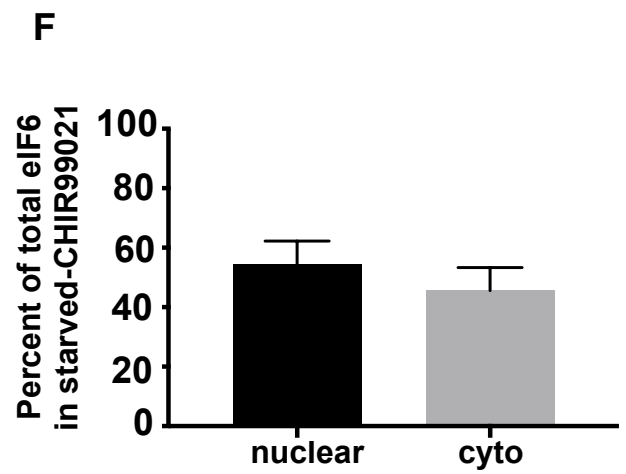
F
Percent of total eIF6 in starved-CHIR99021
100
80
60
40
20
0
nuclear
cyto